A Structured Approach to Defining Active Suspension Requirements

Ashwin M Rao

Thesis submitted to the faculty of the Virginia Polytechnic Institute and State University in partial fulfillment of the requirements for the degree of

Master of Science
In
Mechanical Engineering

Steve Southward (Chair)
Mehdi Ahmadian
Corina Sandu

July 15th, 2016
Blacksburg, VA

Keywords: Active Suspension, Ideal Control Force, Quarter-car, LMS, Road Obstacle

A Structured Approach to Defining Active Suspension Requirements

Ashwin M Rao

ABSTRACT

Active suspension technologies are well known for improving ride comfort and handling of ground vehicles relative to passive suspensions. They are ideally suited for mitigating single-event road obstacles. The work presented in this thesis aims to develop a structured approach for finding the peak force and bandwidth requirements of actuators for active suspensions, to mitigate single-event road obstacles. The approach is kept general to allow for application to different vehicle models, ride conditions and performance objectives. The current state-of-art in active suspensions was first evaluated. Based on these findings, the objectives of the simulation models and approach was defined. A quarter-car model was developed in Matlab to simulate the behavior of active suspensions over unilateral boundary conditions due to different road obstacle profiles. The obstacle profiles were obtained from existing standards and literature and then processed to replicate the interaction of tires on road. A least-mean-squares (LMS) algorithm for adaptive filtering, with the help of look-ahead preview was used to determine the ideal control force profile to achieve the performance objective of the active suspension. A case study was conducted to determine the requirements of the actuator in terms of bandwidth and peak force for different single-event road obstacle profiles, vehicle speeds and look-ahead preview distances. The results of the study show that the vehicle velocity and type of road obstacle have a strong influence on the required peak force and bandwidth of the actuator, while look-ahead preview will be much more important for real time controller implementation.

Acknowledgements

I would like to thank my academic advisor Dr. Steve Southward for giving me the opportunity to work on this research and the guidance to complete my thesis. His courses on Applied Linear Systems and Control were two of my favorite courses at Virginia Tech and gave me the theoretical and practical foundation to solve the problems I encountered during my research.

I would also like to thank Dr. Mehdi Ahmadian and Dr. Corina Sandu for their participation in my thesis committee and taking the time to evaluate my work.

I would like to thank my roommates, friends and all the people of Virginia Tech for making my time in a place halfway around the globe from my home, both enjoyable and memorable. I cherish every day in this wonderful university and country.

Most of all, I want to thank my parents for their support and encouragement throughout my education and graduate studies which allowed me to excel academically and overcome all the obstacles I encountered in my life.

Table of Contents

List of Figures

List of Tables

1 Introduction

This chapter provides motivation for the research presented in this thesis by describing the difficulties in developing active suspensions and deficiency in prior art. Next, the objectives to achieve the goals of this study are explained along with the approach. The chapter ends with an outline of the thesis.

1.1 Background

Active suspensions have been the subject of extensive research for many years to improve the well-known trade-off between ride comfort and handling. Ride comfort can be increased with high damping at low frequencies to prevent bounce, roll and pitch, and lower damping at high frequencies to prevent ride harshness. Improved handling however, requires stiffer springs and dampers at all frequencies to provide good road-holding ability. These conflicting requirements are very difficult to achieve with passive suspensions since they can only temporarily store or dissipate energy at a constant rate. The difficulty is further increased by the fact that the suspension requirements change with different road/speed conditions over which the vehicle operates and therefore, compromises have to be made in passive suspension design to be more widely applicable.

Active suspensions can supply and modulate the flow of energy, generating forces which do not depend on energy previously stored by the suspension and therefore design goals such as ride comfort and handling can be better resolved. They are ideally suited for mitigating single-event road obstacles such as potholes since they can be adapted to instantaneous operating conditions measured by sensors and change their characteristics accordingly.

1.2 Motivation

Since active suspensions can be adapted to different operating conditions, considerable research has been conducted on developing active suspension models and control laws. The state of the art in active suspension control systems have been reviewed by Tseng and Hrovat [1] and it was observed that one of the main challenges for widespread usage of active suspensions still lies in the area of actuator design and implementation. Advances in active and semi-active suspension design will mainly come from improvements in

hardware and control software along with comprehensive use of preview information. The focus in past research on active suspension control has been on the development of real-time control laws which are practically realizable and suitable for a range of road conditions for wider applicability. However, there has been little research on determining the ideal control effort for a known road profile, especially single-event road obstacles. This would be useful for studying the influence of road conditions on the selection of actuators with specific focus on requirements such as peak actuation force and bandwidth.

1.3 Objectives

This work aims to develop a structured approach for determining the peak force and bandwidth requirements for actuators in active suspensions by determining the ideal control force profile required to mitigate single-event road obstacles. The approach is generalized to allow for different vehicle parameters and road/speed conditions. Different control goals including handling, ride comfort and rattle space limitation can be pursued using this approach.

This research has the following requirements:

- A vehicle model well suited to determine the ideal control effort for known road obstacles.
- The use of road obstacle profiles from standards and past research for simulation.
- Implementation of an adaptive filtering technique to determine the ideal control force profile required for an active suspension to mitigate a known road obstacle.
- A case study of the response of the vehicle model under different test conditions to determine peak force and bandwidth requirements of actuators.

1.4 Approach

A linear quarter-car model having an ideal actuator with unlimited authority and bandwidth was developed. A database of single-event road obstacle profiles was gathered from existing standards and literature. A multi-step process was then used to convert these obstacle profiles to unilateral boundary conditions for simulation using the quarter-car model. A strategy was then developed for mathematically determining the ideal control force profile to mitigate single-event road obstacles. A case study was conducting by

simulating the response of the quarter-car under different test conditions. Finally, the results of this study were used to extract the peak force and bandwidth requirements of actuators for active suspensions.

In anticipation of a real-time implementation, preview control was considered in this work. In this scheme, the input from road irregularities is assumed to be measured in front of the vehicle and this information is used by the controller to prepare the system for an oncoming input.

1.5 Outline

The following is a brief outline of the chapters to come. Chapter two provides the background for the study, which includes a literature review of active suspension development and control techniques. Chapter three describes the suspension model that will be used to run simulations along with the assumptions made. Chapter four describes how the unilateral boundary conditions for the suspension model were obtained. Chapter five describes the optimization method used to obtain the control force profile for every simulation of the suspension model. Chapter six presents a case study of the simulations run for different road obstacle profiles. Finally, the thesis ends with the conclusions and recommendations provided in chapter seven.

2 Literature Review

In this chapter, the current state-of-art in active vehicle suspension design and control is reviewed. The chapter begins with a survey of active suspensions and control strategies. This will lay the groundwork for defining the need for, and objectives of the research presented in this thesis.

2.1 Active Vehicle Suspensions

The system design for road vehicle suspensions has been reviewed by Sharp and Crolla [2] to give a broad overview of the different types of suspensions, their performance criteria and modeling without much emphasis on the control strategies and actuator design. It has been well established that active suspensions are capable of providing better performance than passive and semi-active suspensions for any given control objective. Tseng and Hrovat [1] gave a good overview of the design of active suspensions and the tradeoffs between conflicting requirements. Extensive research has been conducted on actuator design for active suspensions, including electromagnetic actuators [3, 4] and hydraulic actuators [5]. It was observed that peak force and bandwidth are the key requirements to be considered while designing actuators for active suspensions. It was also observed that the control systems were only used to evaluate the performance of actuators and not as a design tool for the selection of actuators based on requirements such as peak force and bandwidth.

Research has been conducted on various active suspension control techniques including the use of optimal control, fuzzy control, neural networks, $H\infty$ and preview control. These have been reviewed in [6]. Thompson [7] demonstrated the use of optimal control to optimize a realistic performance index, which places constraints on vehicle response to random road excitation. Ting, Li [8] demonstrated the design of a fuzzy controller for active suspensions. Compared to conventional control theory, fuzzy control relies on control rule sets, which are adopted from expert knowledge and are human dependent. Nguyen, Bui [9] explored hybrid control using $H\infty$ to guarantee robustness of the system and adaptive controls to handle the non-linearity of actuators. However, in all these control methods, the main goal was to improve the trade-off between ride comfort and road

holding. There was no attempt to determine the ideal control effort for a known profile and to use the results for the selection of actuators for active suspensions.

The performance of these control methods were evaluated using road surface profiles that are characterized by their frequency domain properties which are easier to measure and catalogue than amplitude vs time data [10, 11]. However, such a description of road profiles does not account for the effects of single-event obstacles such as road damage, speed humps and potholes. Knowledge of the road profile was assumed to be unknown and therefore the control methods were designed to provide good performance on typically expected road conditions.

Preview information has been considered in the work presented in this thesis. It was first proposed by Bender [12] who showed that preview information can provide significant improvements in active suspensions. Tomizuka [13] showed that the form of preview control depends on the roadway spectrum and on the vehicle speed. The preview can be either obtained with sensors in the front of the vehicle or by considering the input to the rear wheels as a delayed version of the input to the front wheels of the vehicle [14] or even from the lead vehicle in a convoy [15]. Wiener Filter theory and Discrete Linear Quadratic Regulator theory has been used to develop control strategies making use of preview information in most of the preceding research. Preview can not only improve ride comfort but also reduce power requirements [16]. The preview control implemented in the mentioned research is mainly targeted at real time application, whereas, in the work presented in this thesis, preview was used offline and iteratively.

2.2 Road Profiles

Since the evaluation of active suspension control schemes is mainly done through simulation, the road profiles which provide input to suspension models have been thoroughly studied [10, 11]. Agostinacchio, Ciampa [17] demonstrated the use of harmonic functions to generate random road profiles according to the ISO 8608 standard. Schmeitz [18], [19] demonstrated the use of elliptical tandem cams to filter road profiles before using them as inputs for simulation.

2.3 Adaptive Filtering

In this work, rather than develop real-time control laws or algorithms, the focus was on the determining the ideal control force profile. This was done by offline simulation of active suspensions with optimization for specific road obstacle profiles without concern for how the results would be achieved in real-time. This has been done through adaptive filtering.

Methods of adaptive filtering have been well established for application that do not involve vehicle suspensions [20]. They have also been applied to system identification for active suspensions [21], however they have not been used as a method of offline optimization for active suspension control.

3 System Model

Computer simulations are a convenient and effective method of evaluating vehicle suspensions. It has been established from many studies that the most significant and insightful conclusions for vehicle suspensions can be observed from a simple quarter-car model [2]. A quarter-car model is used to develop a proof of concept for the method used in this research to determine active suspension requirements. The results obtained from analysis of the quarter-car model can then be used in further investigation using higher degree of freedom models.

3.1 Assumptions

The following assumptions are made while developing the quarter car model for active suspension control simulation.

- The outputs of the model are chosen to be the acceleration of the sprung mass and the relative displacement between the sprung and unsprung mass. This can be performed practically with the help of an accelerometer and displacement sensor.
- It is assumed that the actuation force generator in the model is ideal, having an unlimited bandwidth and authority. This is assumed so that the simulation results are not limited by the force generator.
- A linear model is assumed so that a proof of concept can be obtained. The results of the simulations can be used in further investigation with more complex non-linear models.
- The tire-ground interface is a unilateral boundary condition such that the road profile provides the input to the model, but is not affected by the reaction forces generated by the model.
- The tire of the quarter car is always in contact with the road profile and there is no lift-off.
- The tire of the model is assumed to be in contact with an effective road profile, which is obtained by pre-processing an actual point-cloud road profile.

3.2 Model Description

The quarter car model is used to simulate the response of a vehicle's suspension to inputs due to the road on which the vehicle is being driven.

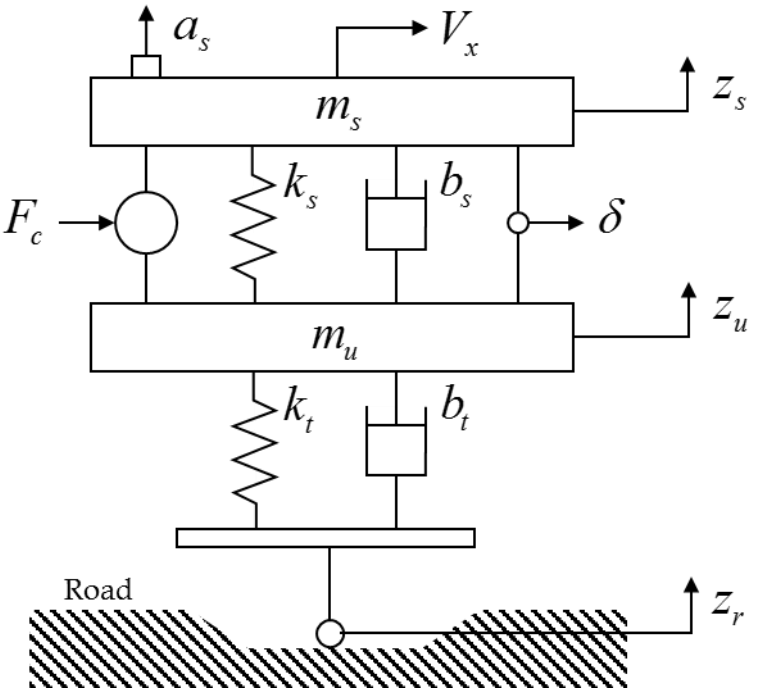

Figure 3.1: Quarter-car model

Figure 3.1 shows a schematic diagram of the quarter-car model. m_u, m_s are the unsprung mass and sprung mass respectively, k_t, k_s are the spring constants of the tire and the suspension respectively, b_t, b_s are the damping coefficients of the tire and the suspension respectively. z_r is the vertical displacement as a result of the road profile. z_u, z_s are the vertical displacement of the unsprung and sprung mass respectively. a_s is the sprung mass acceleration and δ is the relative displacement between the sprung and unsprung mass. F_c is the control force.

The quarter car model is derived with inputs ($\dot{z}_r$ and F_c) and outputs (a_s and δ). It should be noted that vertical velocity $\dot{z}_r$ is used instead of vertical displacement z_r . This

is done since the tire is modeled with a damper and would require a velocity input. This prevents undamped oscillations in the tire. It also ensures that a constant absolute vertical displacement due to a road profile does not behave as a constant excitation.

The equations of motion of the quarter-car model can be obtained using free body diagrams for the equilibrium position.

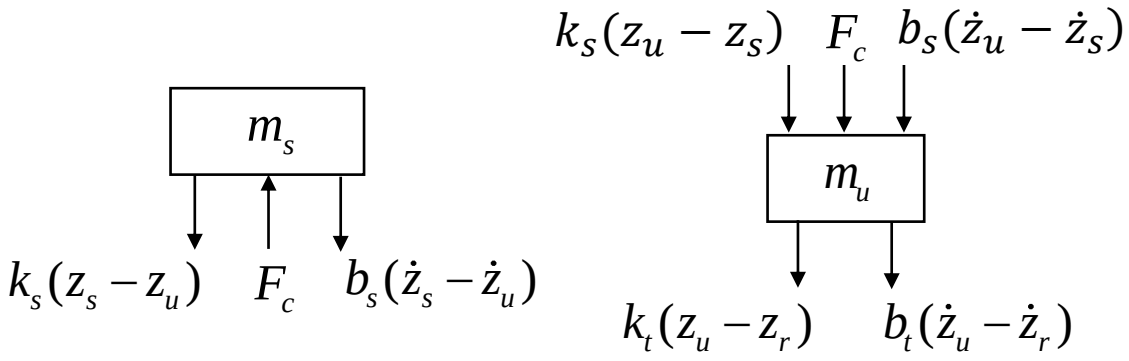

Figure 3.2: Free body diagram of (a) sprung mass, (b) unsprung mass

Figure 3.2 shows the free body diagrams used to obtain the equilibrium equations to describe the quarter-car model.

$$m_s\ddot{z}_s = -k_s(z_s - z_u) - b_s(\dot{z}_s - \dot{z}_u) + F_c \tag{3.1}$$

$$m_u\ddot{z}_u = -k_s(z_u - z_s) - k_t(z_u - z_r) - b_s(\dot{z}_u - \dot{z}_s) - b_t(\dot{z}_u - \dot{z}_r) - F_c \tag{3.2}$$

Equations (3.1) and (3.2) are the equilibrium equations for the quarter-car model. These equations are used to obtain the state-space representation of the quarter-car.

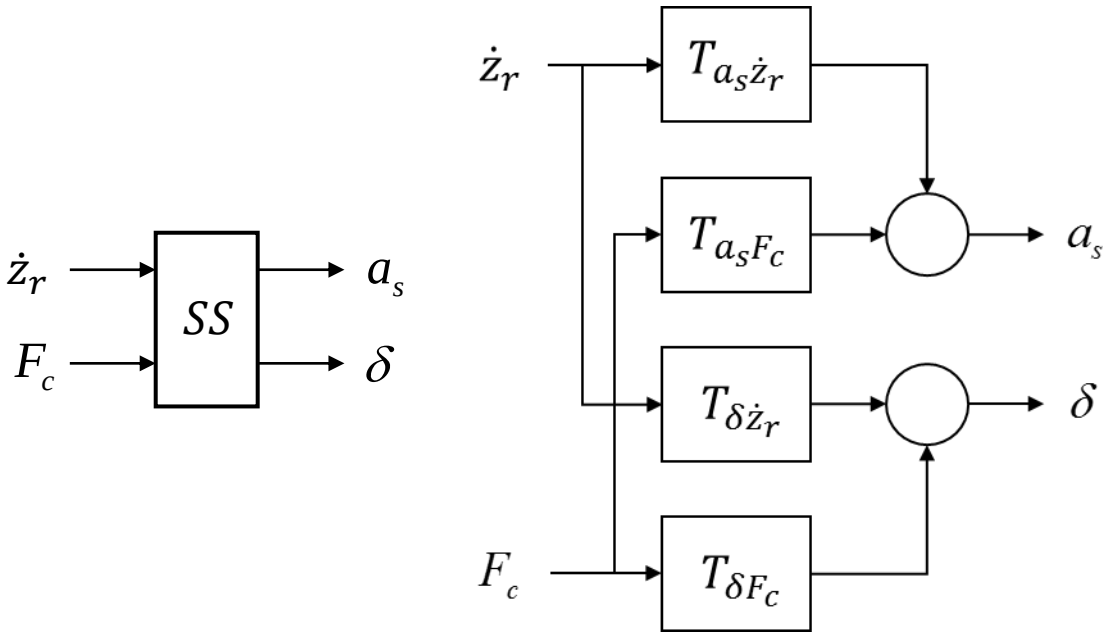

Figure 3.3: Inputs and outputs of quarter-car model

The state-space model is shown pictorially in Figure 3.3 where $T_{a_s\dot{z}_r}$, $T_{a_sF_c}$, $T_{\delta\dot{z}_r}$ and $T_{\delta F_c}$ are the input output transfer functions.

$$\begin{aligned} x_1 &= z_s \\ x_2 &= \dot{z}_s \\ x_3 &= z_u \\ x_4 &= \dot{z}_u \\ x_5 &= z_r \end{aligned} \tag{3.3}$$

Equations in (3.3) show the chosen states for the state-space representation. It should be noted that vertical displacement due to the road profile is selected as a state and not an input.

$$
\begin{aligned}
\dot{x}_1 &= x_2 \\
\dot{x}_2 &= x_1\left(\frac{-k_s}{m_s}\right) + x_2\left(\frac{-b_s}{m_s}\right) + x_3\left(\frac{k_s}{m_s}\right) + x_4\left(\frac{b_s}{m_s}\right) + \frac{F_c}{m_s} \\
\dot{x}_3 &= x_4 \\
\dot{x}_4 &= x_1\left(\frac{k_s}{m_u}\right) + x_2\left(\frac{b_s}{m_u}\right) + x_3\left(\frac{-k_s - k_t}{m_u}\right) + x_4\left(\frac{-b_s - b_t}{m_u}\right) + x_5\left(\frac{k_t}{m_u}\right) + \dot{z}_r\left(\frac{b_t}{m_u}\right) - \frac{F_c}{m_u} \\
\dot{x}_5 &= \dot{z}_r
\end{aligned}
\tag{3.4}
$$

The equations in (3.4) are the state-space equations for the quarter car model.

$$
\begin{Bmatrix} \dot{x}_1 \\ \dot{x}_2 \\ \dot{x}_3 \\ \dot{x}_4 \\ \dot{x}_5 \end{Bmatrix} =
\begin{bmatrix}
0 & 1 & 0 & 0 & 0 \\
\frac{-k_s}{m_s} & \frac{-b_s}{m_s} & \frac{k_s}{m_s} & \frac{b_s}{m_s} & 0 \\
0 & 0 & 0 & 1 & 0 \\
\frac{k_s}{m_u} & \frac{b_s}{m_u} & \frac{-k_s - k_t}{m_u} & \frac{-b_s - b_t}{m_u} & \frac{k_t}{m_u} \\
0 & 0 & 0 & 0 & 0
\end{bmatrix}
\begin{Bmatrix} x_1 \\ x_2 \\ x_3 \\ x_4 \\ x_5 \end{Bmatrix} +
\begin{bmatrix}
0 & 0 \\
0 & \frac{1}{m_s} \\
0 & 0 \\
\frac{b_t}{m_u} & \frac{-1}{m_u} \\
1 & 0
\end{bmatrix}
\begin{Bmatrix} \dot{z}_r \\ F_c \end{Bmatrix}
$$

$$
\begin{Bmatrix} y_1 \\ y_2 \end{Bmatrix} =
\begin{bmatrix}
\frac{-k_s}{m_s} & \frac{-b_s}{m_s} & \frac{k_s}{m_s} & \frac{b_s}{m_s} & 0 \\
1 & 0 & -1 & 0 & 0
\end{bmatrix}
\begin{Bmatrix} x_1 \\ x_2 \\ x_3 \\ x_4 \\ x_5 \end{Bmatrix} +
\begin{bmatrix}
0 & \frac{1}{m_s} \\
0 & 0
\end{bmatrix}
\begin{Bmatrix} \dot{z}_r \\ F_c \end{Bmatrix}
\tag{3.5}
$$

$$
\begin{aligned}
\{\dot{x}\} &= [A]\{x\} + [B]\{u\} \\
\{y\} &= [C]\{x\} + [D]\{u\}
\end{aligned}
\tag{3.6}
$$

The equations (3.5) and (3.6) give the state-space representation in matrix form.

These equations were entered into Matlab to allow the model to be simulated.

Table 3.1: Parameter values for quarter-car model

Parameter	Value	Unit
m_s	400	kg
m_u	40	kg
k_s	21000	N/m
k_t	150000	N/m
b_s	1500	Ns/m
b_t	250	Ns/m

The values for the parameters of the quarter-car model are shown in Table 3.1. They were chosen to be representative of a typical passenger vehicle.

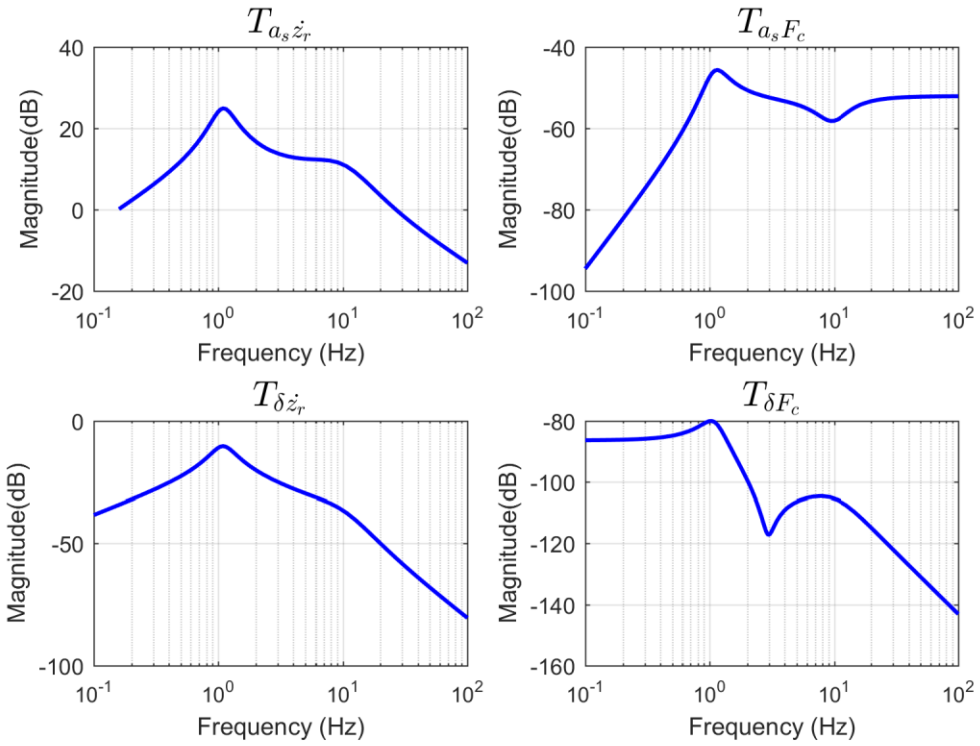

Figure 3.4: Transfer functions of quarter-car model

Figure 3.4 shows the transfer functions for each path of the quarter-car with the chosen parameters. The natural frequencies of the quarter car model are approximately 1 and 10

Hz. The code was developed in Matlab to be general and allows easy modification of these parameters to test different vehicle models ranging from sedans to trucks.

4 Unilateral Boundary Conditions

The unilateral boundary conditions are used to simulate the behavior of the developed suspension model on different types of road obstacles. Extensive research has been conducted on road obstacle profiles and their interaction with a vehicle. There are also standards describing their geometries. Existing research on active suspension control has focused more on arbitrarily simulated inputs. The work presented in this thesis takes advantage of the available road obstacle profile data in existing literature. In this way, any newly measured profiles can be easily simulated to provide insights into designing vehicle suspensions for it.

A multi-step process was used to convert road obstacle profile geometries to unilateral boundary conditions that are suitable for simulation using the quarter-car model. The following steps were taken:

a) Discretization of displacement profiles in Matlab
b) Addition of unevenness
c) Tandem Elliptical Cam pre-processing
d) Low-pass filtering
e) Differentiation to obtain velocity profiles

4.1 Road Obstacles

The input to the quarter-car model is in the form of vertical velocity as a function of time due to different road obstacle profiles. There are a vast number of road obstacles that could be simulated; however, the following general types of road obstacles were evaluated to provide representative results:

- Curbs
- Speed Humps
- Potholes
- Uneven Road

4.1.1 Curbs

A curb is the edge where a sidewalk meets a street or another roadway. They serve multiple functions including the separation of road from roadside, support the pavement edge, and discouraging drivers from parking or driving on sidewalks and lawns.

On higher-speed roadways, curbs can potentially cause drivers to lose control, roll over and crash. There have been a very limited number of full-scale crash tests on curb-barrier combinations and a large percentage have been unsuccessful [22].

There are a number of types of curbs with different shapes, materials and heights. Curbs often have a vertical or near-vertical face that extends 75 to 200 mm above the road surface and are located very near the edge of the traveled way. Figure 4.1 shows some typical standard curb profiles obtained from [22].

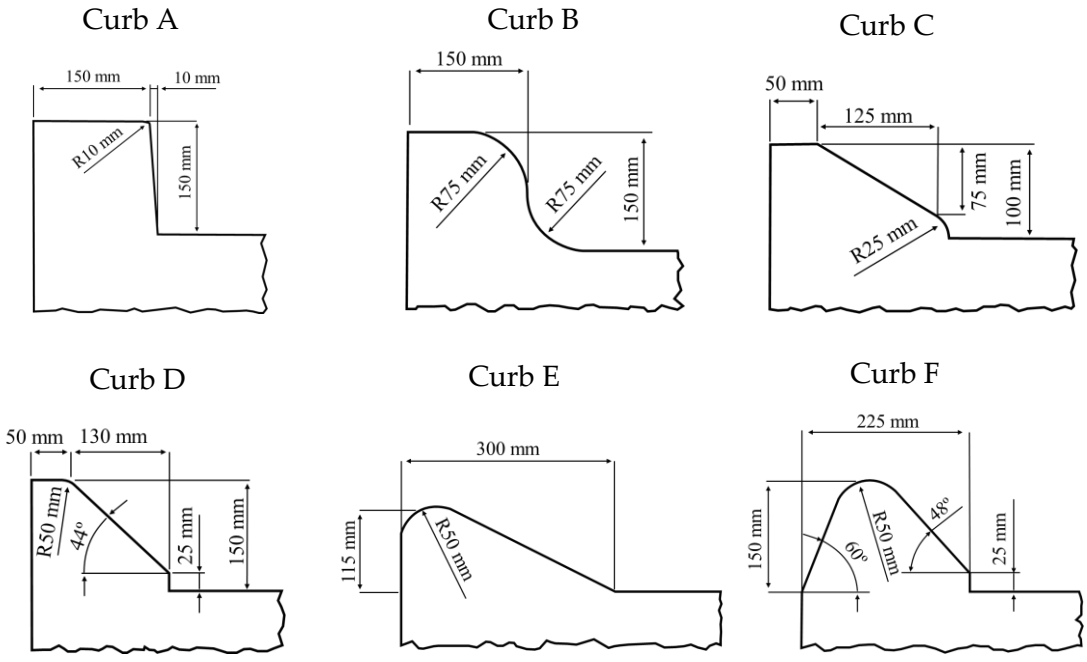

Figure 4.1: Standard curb profiles

Source: Plaxico, C. A., et al. (2005). Recommended Guidelines for Curb and Curb-Barrier Installations. United States: 112p. Used under fair use 2016.

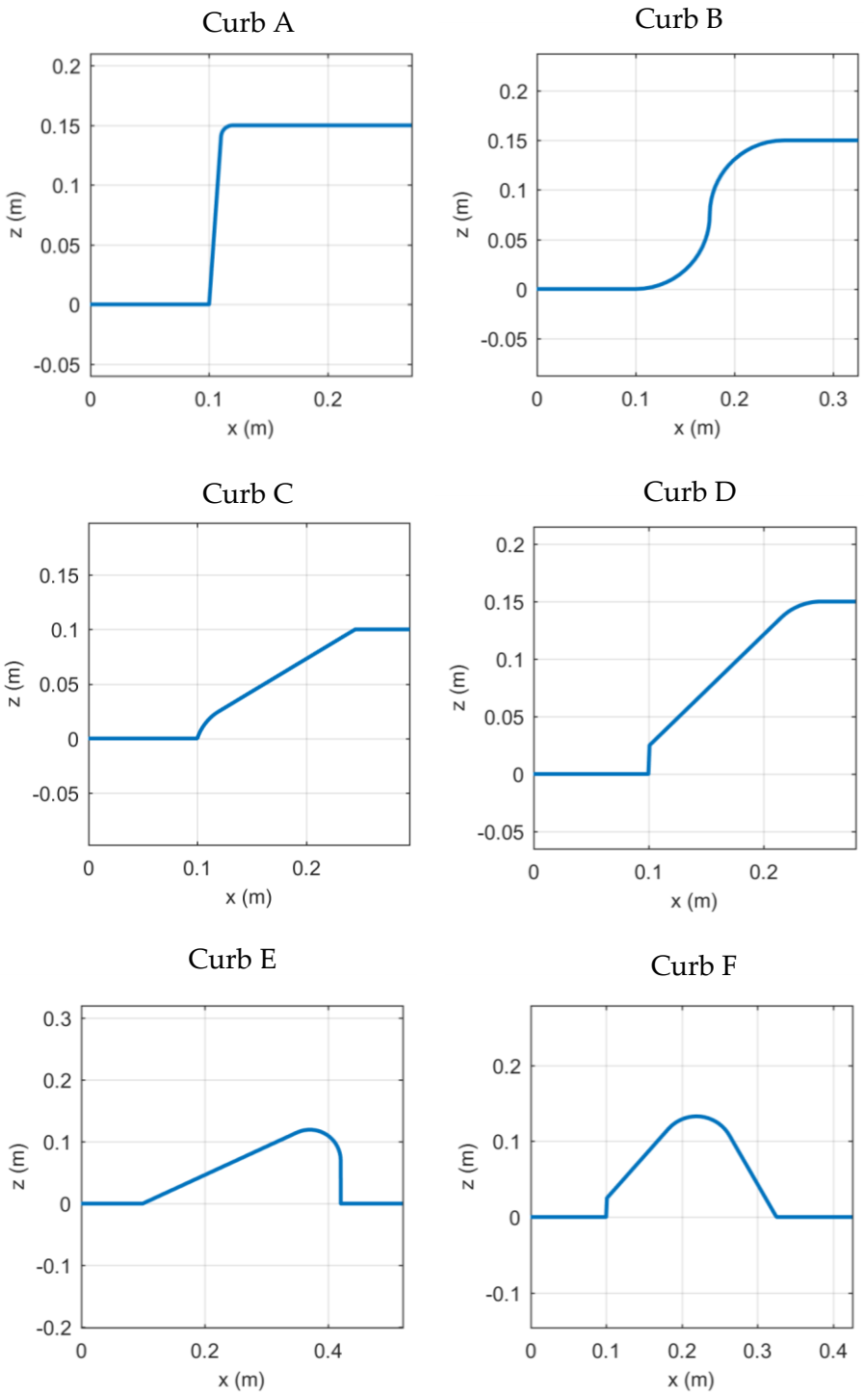

Figure 4.2: Standard curb profiles in Matlab

Figure 4.2 shows the curb profiles that were discretized using Matlab for simulation in the form of vertical displacement corresponding to distance travelled. They were generated by selecting grid points from the geometry of the profile and joining these points with straight lines.

4.1.2 Speed Humps and Speed Bumps

A speed hump is a raised area in the roadway extending laterally across the travel way. Most agencies implement speed humps with a height of 76 to 90 mm and a travel length of 3.7 to 4.3 m. They are generally used on residential local streets.

Speed bumps on the other hand are found on private roadways and parking lots and do not tend to exhibit consistent design parameters from one installation to another. They generally have a height of 76 to 152 mm and a travel length of 0.3 to 1 m. [23].

Speed bumps and speed humps have critically different impacts on vehicles. Speed bumps cause significant discomfort even at typical residential operational speed ranges.

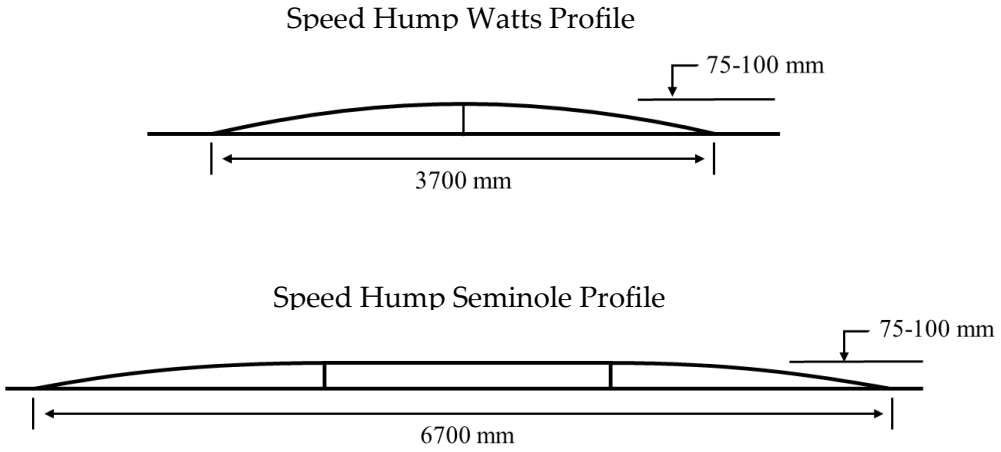

Figure 4.3: Speed hump profiles

Source: Weber, P. A. and J. P. Braaksma (2000). "Towards a North American geometric design standard for speed humps." ITE Journal (Institute of Transportation Engineers) 70(1): 30-34. Used under fair use 2016.

Two common speed hump profiles are the Watts Profile and Seminole Profile shown in Figure 4.3. The Watts Profile is a section of a cylinder 3.7 meters long and 75 to 100 mm height extending over the width of the street. Most vehicles can traverse them safely at 25

to 30 kilometers per hour (km/h). The Seminole Profile or “flat top” hump features the addition of a 3 m flat section into a Watts Profile hump for an overall length of 6.7 m [24].

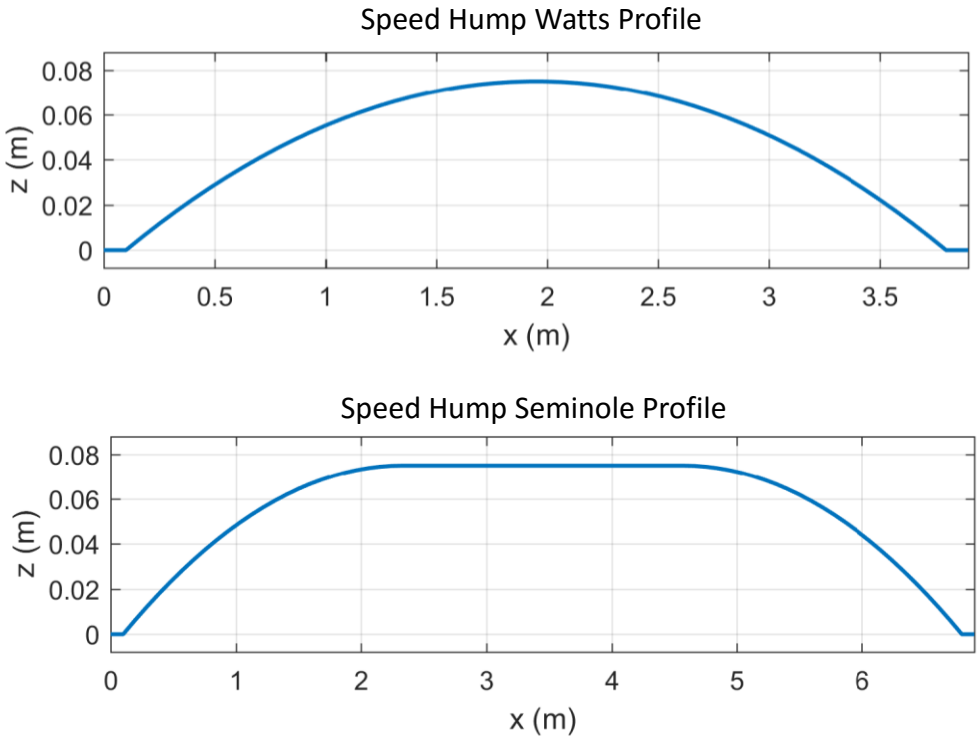

Figure 4.4: Speed hump profiles in Matlab

Figure 4.4 shows the standard speed hump profiles that were discretized in Matlab for simulation.

4.1.3 Potholes

Potholes are a type of failure in asphalt pavement caused by the presence of water in the underlying soil structure and presence of traffic passing over the affected area.

Potholes can grow to several feet in width, though they usually only develop to depths of a few inches. If they become large enough, they can cause damage to tires, wheels and vehicle suspensions and also road accidents.

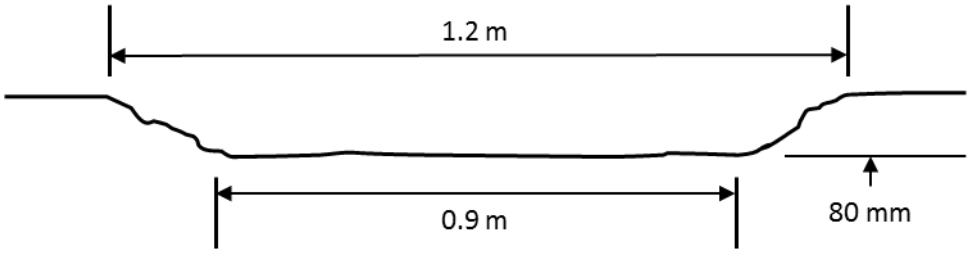

Figure 4.5: Pothole profile

Figure 4.5 shows a typical pothole profile. Potholes can be of very different shapes, sizes and geometrical properties. To the author's knowledge, there are no standards for pothole classification based on size and dimensions other than a description of severity based on depth [25]. For this reason, pothole profile dimensions obtained through experimentation in [26] were used for simulations.

Table 4.1: Specimen pothole dimensions

Source: Tiong, P. L. Y., et al. (2012). "Road surface assessment of pothole severity by close range digital photogrammetry method." World Appl Sci J 19(6): 867-873.

Specimen Name	Diameter (m)	Area (m^2)	Depth (mm)
P1	0.575	0.26	79
P2	0.400	0.13	60
P3	1.250	1.23	96
P4	0.915	0.37	59
P5	0.886	0.28	75
P6	1.240	1.21	96
P7	0.915	0.37	59
P8	0.866	0.28	75
P9	0.757	0.45	89
P10	0.556	0.24	90

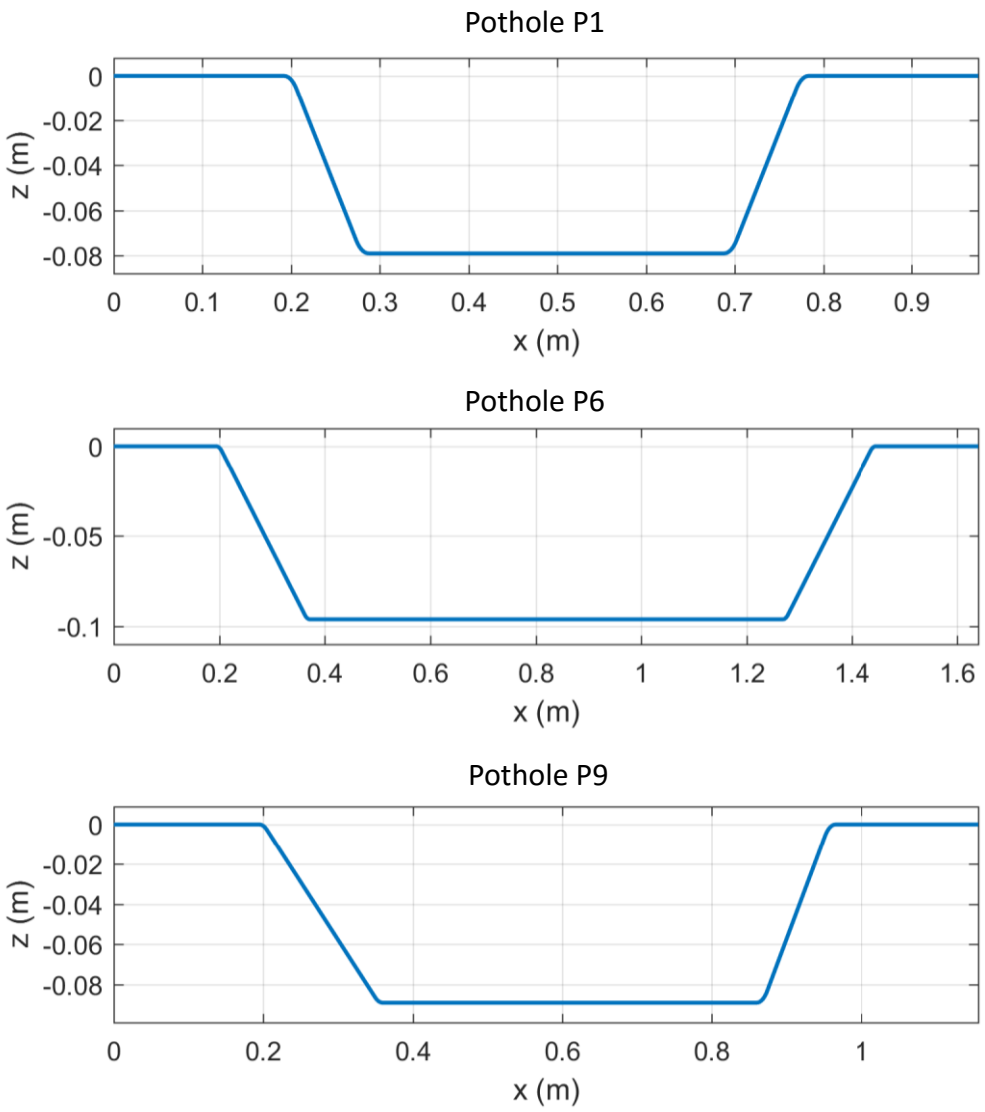

Figure 4.6: Pothole profiles in Matlab

Figure 4.6 shows the pothole profiles discretized in Matlab using the dimensions from Table 4.1 for P1, P6 and P9. Potholes can have very uneven surfaces which are not captured by these dimensions. Therefore, they were used to develop an overall geometry and road unevenness was added in Matlab by a method that will be discussed in the next section.

4.1.4 Uneven Road Profile

Road unevenness is the deviation from planar and smooth surface affecting the vehicle/tire interaction. It is measured using prophilometry. These measurements are used to classify the road unevenness using two general approaches [27].

The first approach is to evaluate the road unevenness based on the reasoning that what is important for a user of the road is the knowledge of the effects which unevenness causes on the traversing vehicle and not the knowledge of the unevenness alone. Several measuring devices were developed to provide an International Roughness Index (IRI). Obtaining the IRI involves the measurement of elevations along a road section at equally spaced distance points, evaluation of the local slopes and input into a two-mass model simulating a standard reference vehicle. The response data is filtered and the mean value of slopes gives the IRI.

The second description of the road is in terms of the geometry of the elevation change in dependence on the track distance, or longitudinal profile. The longitudinal profile is considered to be a realization of a random function and the power spectral density (PSD) is assumed to be its simplest form. The advantage of this method is that, once the PSD characteristics are obtained, they can be used to create shaping filters that can generate artificial road profiles from random noise, which have the same characteristics of measured road profiles.

The results of the first method are not suitable for input into a quarter-car model, which requires the longitudinal road profile. Therefore, the second method is used for simulation purposes due to the ease and customizability of obtaining road profiles of varying unevenness.

4.1.5 Random Road Profile Generation

Random road profiles of chosen roughness were generated and added to the obstacle profiles to simulate road roughness according to the method used in [17].

ISO Classification

Roads are classified according to the ISO 8608 standard using spatial frequency, road profile and PSD. Spatial frequency or wave number is defined as cycles/meter contrary to the temporal frequency, Hertz (cycles/second). The use of ISO 8608 is based on the assumption that a given road has equal statistical properties everywhere along a section to be classified.

Eight classes of roads are identified from class A to class H where class A includes roads that have a minor degree of roughness and are of good quality while class H includes roads that have a very high degree of roughness and are of very poor quality.

The classes are described by the power spectral density of vertical displacements G_d as a function of spatial frequency n with the conventional value of n_0 = 0.1 cycles/m. In practice, $G_d(n)$ is plotted with a log-log scale.

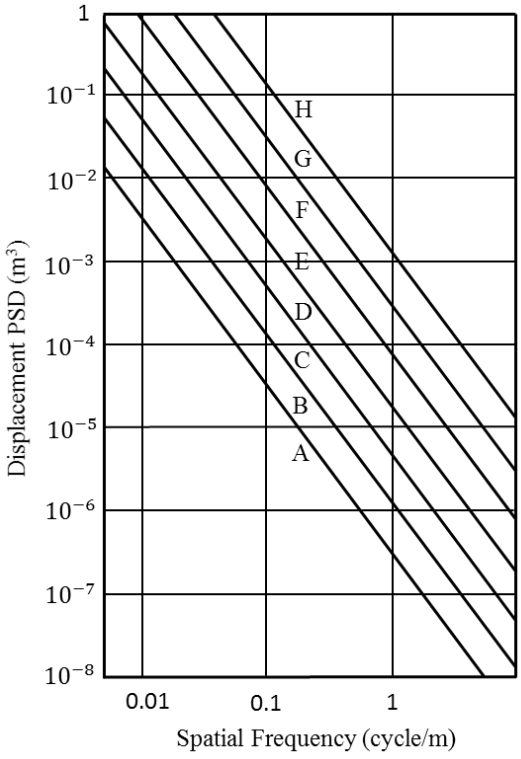

Figure 4.7: ISO 8608 road surface classification

Source: ISO 8608:1995 – Mechanical vibration – Road surface profiles – Reporting of measured data. Used under fair use 2016.

Figure 4.7 shows the log-log plots for different road surface classifications ranging from A (good quality) to H (poor quality).

Table 4.2: ISO 8608 values for different road classes

Road Class	$G_d(n_0)(10^{-6}m^3)$	
	Lower Limit	Upper Limit
A	-	32
B	32	128
C	128	512
D	512	2048
E	2048	8192
F	8192	32768
G	32768	131072
H	131072	-
	n_0 = 0.1 cycles/m	

Table 4.2 shows the ISO 8608 values for different road classes of increasing roughness.

$$h(x) = A_i \cos(2\pi \cdot n_i \cdot x + \varphi) \tag{4.1}$$

Equation (4.1) is used to describe the road profile as a simple harmonic function where A_i is the amplitude, n_i is the spatial frequency and φ is the phase angle.

$$G_d(n_i) = \frac{A_i^2}{2 \cdot \Delta n} \tag{4.2}$$

The power spectral density at a given spatial frequency is given by equation (4.2) where Δn is the frequency band.

$$h(x) = \sum_{i=0}^{N} A_i \cos(2\pi \cdot n_i \cdot x + \varphi) = \sum_{i=0}^{N} \sqrt{2 \cdot \Delta n \cdot G_d(i \cdot \Delta n)} \cdot \cos(2\pi \cdot i \cdot \Delta n \cdot x + \varphi_i) \tag{4.3}$$

Using (4.1) and (4.2) and assuming a random phase angle φ_i following a uniform probabilistic distribution within the $0 - 2\pi$ range, the artificial profile can be described by equation (4.3).

$$
\begin{aligned}
h(x) &= \sum_{i=0}^{N} \sqrt{\Delta n} \cdot 2^{k} \cdot 10^{-3} \cdot \left(\frac{n_0}{i \cdot \Delta n} \right) \cdot \cos(2\pi \cdot i \cdot \Delta n \cdot x + \varphi_i) \\
\Delta n &= 1/L \\
n_{\max} &= 1/B \\
N &= n_{\max} / \Delta n = L/B
\end{aligned}
\tag{4.4}
$$

An artificial road profile of length L from ISO classification can be generated by equation (4.4) where x is the abscissa variable form **O** to L. N is the number of intervals in special frequency and k is a constant value depending on the ISO road profile classification assuming integers increase from 2 to 9 corresponding to profiles from class A to class H. n_0 = 0.1 cycles/m.

Table 4.3: k values for different ISO road classes

Road Class	k value
A	2
B	3
C	4
D	5
E	6
F	7
G	8
H	9

Table 4.3 shows different ISO road classes and their corresponding k values.

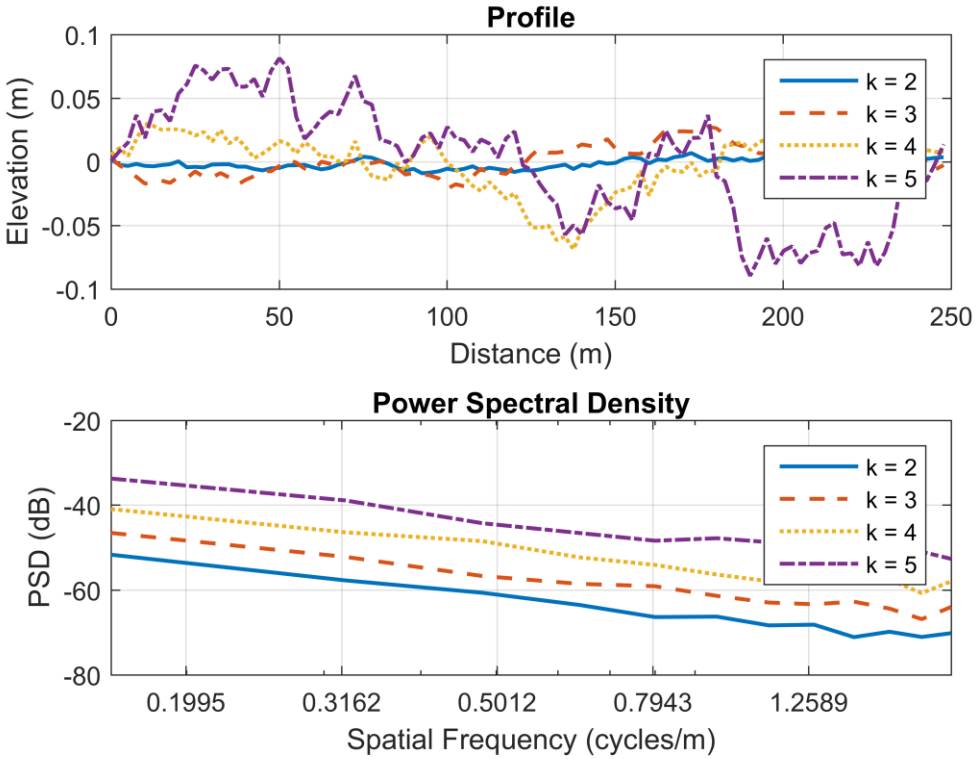

Figure 4.8: Random road profiles generated in Matlab

Figure 4.8 shows some random road profiles generated using this method. The road profiles were generated in Matlab and can be used as input for the quarter car model. It is seen that the PSDs of the generated profiles are similar to those of the ISO 8608 classification. A low value of k results in smoother profile than a high value of k.

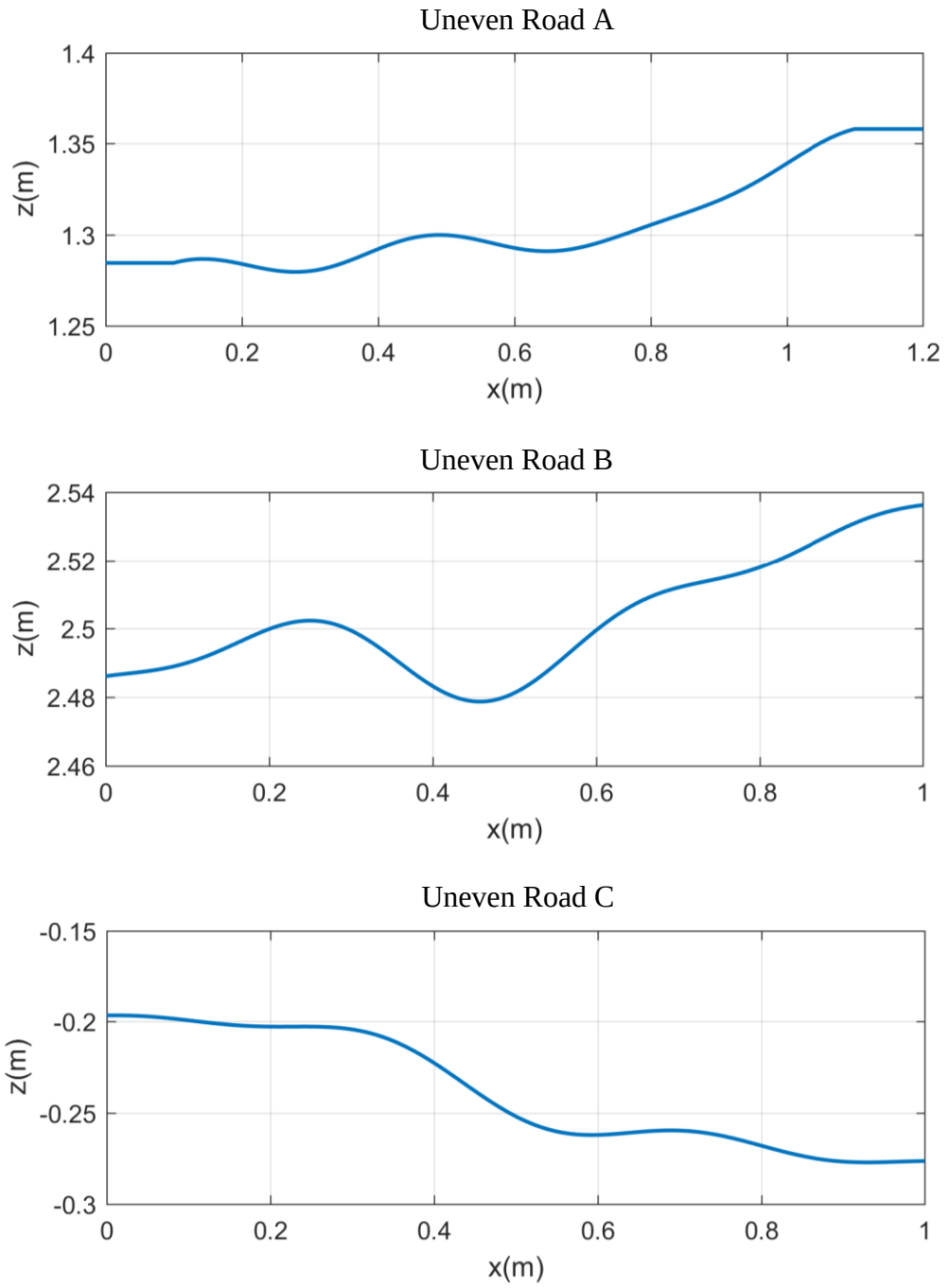

Figure 4.9: Uneven road profiles

Using this method, Class A road unevenness was added to every standard road profile to increase the realism of the simulation results. Random single-event obstacles were also developed using a high k value of seven to represent very harsh road profiles of class F

to be tested by themselves. Figure 4.9 shows the uneven road obstacle profiles created in Matlab for simulation.

4.2 Pre-processing Road Profiles

The road obstacle profiles serve as input to the quarter-car model through the tire. If the wavelength is smaller than two or three times the contact length and the model is assumed to contact the road at a single point, geometric filtering of the profile becomes necessary. This is done to account for the enveloping of obstacles at the contact patch.

4.2.1 Tandem Elliptical Cam Pre-Processing

The 'Tandem Elliptical Cam Technique' as described in [18] was used to process the road profile, and parameter values were obtained from [19]. This enveloping model moves over the actual road surface and generates an effective road surface description that serves as input to the quarter-car model. Numerous simulation results with measurements have shown the model to be valid in the scope of experiments.

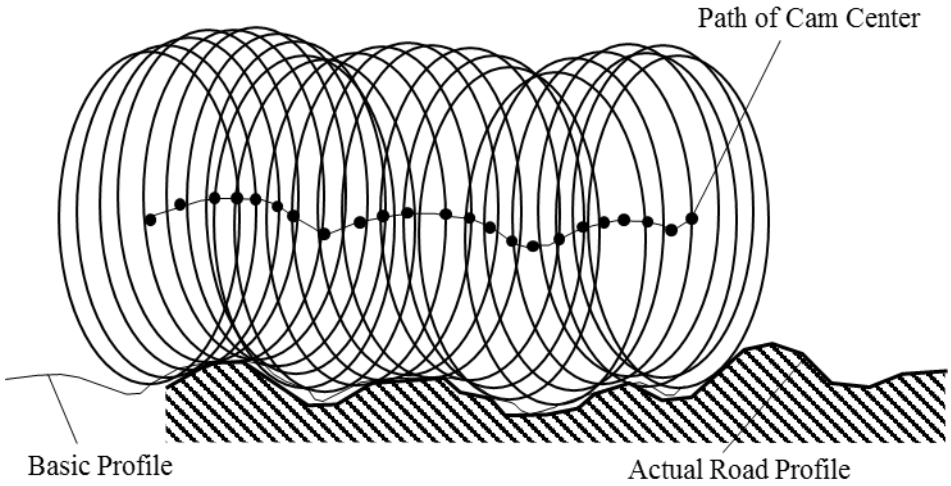

Figure 4.10: Filtering of road profile

Source: Pacejka, H. (2006). Tire and Vehicle Dynamics, Butterworth-Heinemann. Used under fair use 2016.

Figure 4.10 shows the filtering of a road profile and obtaining a basic curve using an elliptical cam. It is seen that the basic curve behaves as a filtered version of the actual road profile.

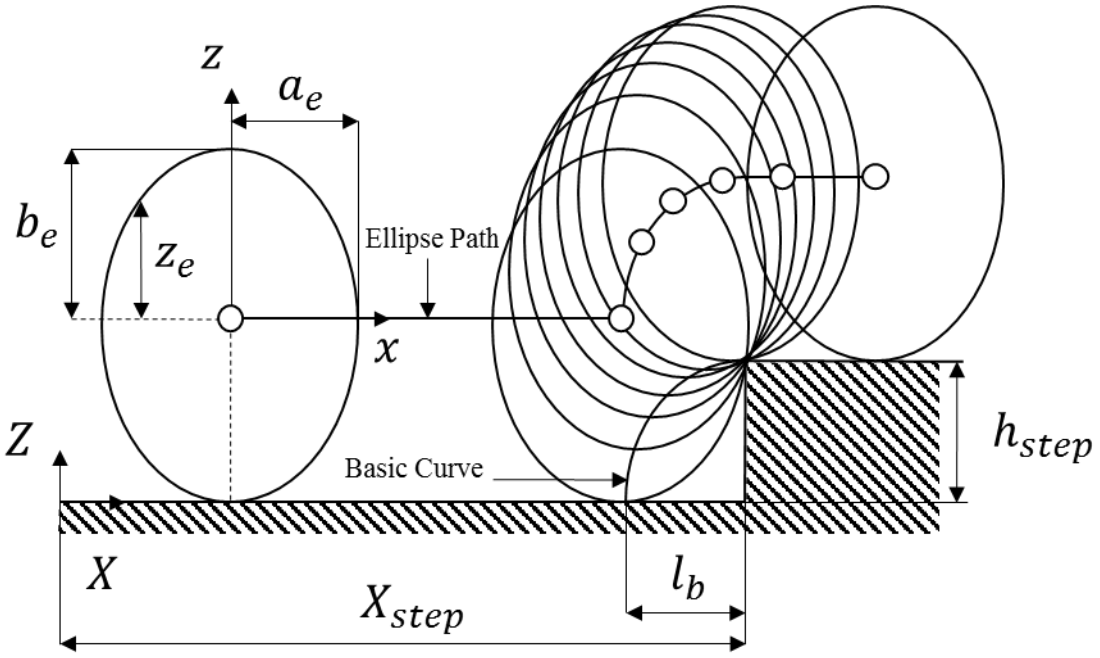

Figure 4.11: Generation of basic curve

Source: Schmeitz, A. J. C. (2004). A Semi-Empirical Three-Dimensional Model of the Pneumatic Tyre Rolling over Arbitrarily Uneven Road Surfaces. Institutional Repository, Delft University of Technology: 320. Used under fair use 2016.

Figure 4.11 shows the generation of the basic curve using an ellipse defined by the shape parameters a_e, b_e and c_e, where c_e is the ellipse exponent. The selection of these shape parameters allows the modeling of different tires in accordance with experimental results. The derivation of the equation for the basic curve is now discussed.

$$\left(\frac{x}{a_e}\right)^{c_e} + \left(\frac{z}{b_e}\right)^{c_e} = 1 \tag{4.5}$$

Equation (4.5) gives the equation of the ellipse in local coordinates x and z.

$$l_b = a_e \left(1 - \left(1 - \frac{|h_{step}|}{b_e} \right)^{c_e} \right)^{\frac{1}{c_e}} \tag{4.6}$$

Equation (4.6) gives the length l_b of the elliptical basic curve where h_{step} is the height of the step.

$$z_e = \left| b_e \left(1 - \left(\frac{|x|}{a_e} \right)^{c_e} \right)^{\frac{1}{c_e}} \right| \tag{4.7}$$

Equation (4.7) gives the distance z_e between the local x-axis and the ellipse.

$$\begin{aligned} Z &= 0 && \text{if} \quad X \le -l_b + X_{step} \\ Z &= h_{step} - b_e + \left| b_e \left(1 - \left(\frac{|X - X_{step}|}{a_e} \right)^{c_e} \right)^{\frac{1}{c_e}} \right| && \text{if} \quad -l_b + X_{step} < X < X_{step} \\ Z &= h_{step} && \text{if} \quad X > X_{step} \end{aligned} \tag{4.8}$$

Equation (4.8) gives the global vertical coordinates Z for the basic curve.

To obtain an effective road profile from an input road profile, two elliptical cams are used in tandem.

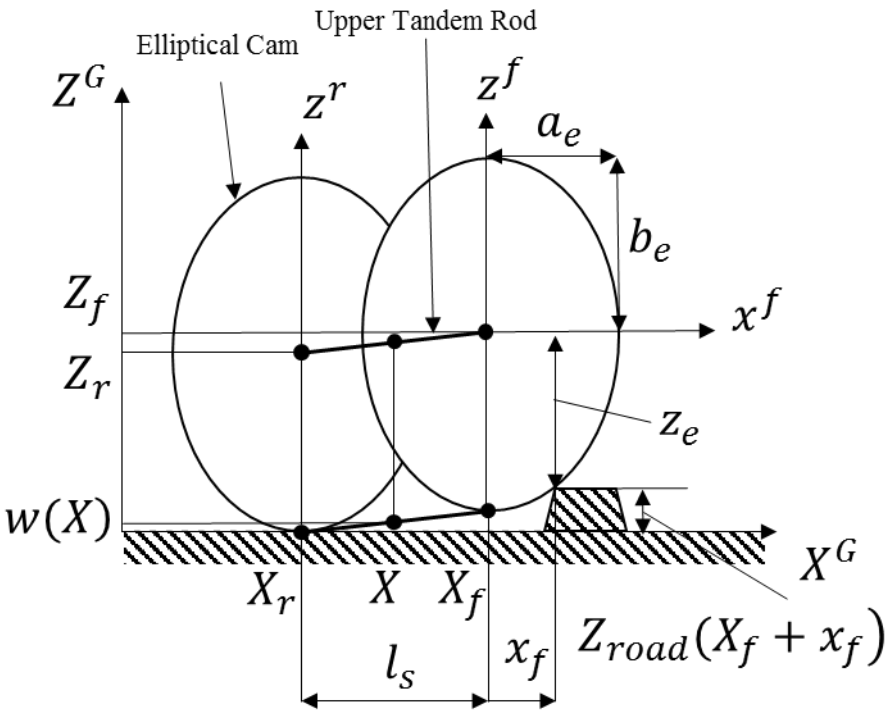

Figure 4.12: Tandem Elliptical Cams

Source: Schmeitz, A. J. C. (2004). A Semi-Empirical Three-Dimensional Model of the Pneumatic Tyre Rolling over Arbitrarily Uneven Road Surfaces. Institutional Repository, Delft University of Technology: 320. Used under fair use 2016.

The Figure 4.12 shows the tandem elliptical cams connected by an upper and lower tandem rod. Upper case letters represent global coordinates while lower case letters represent local coordinates. X_f, Z_f and X_r, Z_r represent the centers of the front and rear ellipse in global coordinates and similarly for the lower case letters.

$$Z_f = \max\left[Z_{road}\left(X_f + x_f \right) + z_e(x_f) \right] \tag{4.9}$$

Equation (4.9) gives the global height of the front ellipse center where Z_{road} is any input road profile defined at distances X_f. The global height of the rear ellipse is calculated in the same way.

$$w(X) = \frac{Z_f + Z_r}{2} - b_e \tag{4.10}$$

Equation (4.10) gives the effective height (w) which equals the midpoint of the lower tandem rod. This equation can be used to obtain the final effective profile for any input road profile.

$$\begin{aligned} p_{ls} &= \frac{l_s}{2a} \\ p_{ae} &= \frac{a_e}{r_0} \\ p_{be} &= \frac{b_e}{r_0} \\ p_{ce} &= c_e \end{aligned} \tag{4.11}$$

Equations (4.11) give the dimensionless parameters which control the length of the tandem rod and shape of the elliptical cam. It is assumed that the tandem base length (l_s) is related to the contact length $(2a)$ of the tire and that the shape of the elliptical cam is related to the free tire radius (r_0).

Table 4.4: Chosen elliptical cam parameters for simulation

Source: Pacejka, H. (2006). Tire and Vehicle Dynamics, Butterworth-Heinemann.

Parameter Description	Symbol	Value
Unloaded Radius	r_o	0.310 m
Effective rolling radius	r_{eo}	0.305 m
Half contact length	a	0.0603 m
Half ellipse length / unloaded radius	p_{ae}	1.0325
Half ellipse height / unloaded radius	p_{be}	1.0306
Ellipse exponent	p_{ce}	1.8230
Shift length / contact length	p_{sh}	0.8773

Table 4.4 gives the chosen elliptical cam parameters for simulation. They can be modified to obtain the effects of different tires and vehicle loads.

The ‘Tandem Elliptical Cam Technique’ can be used to process a road profile and obtain an effective profile that can be used as input to the quarter-car model.

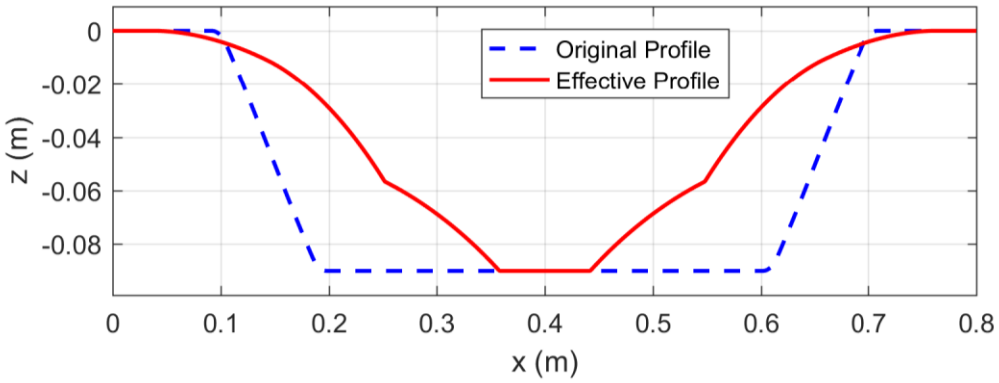

Figure 4.13: Filtering of road profile using tandem elliptical cams

Matlab code was developed to pre-process any input road profile using this technique. Figure 4.13 shows an example of the filtering effect of the 'Tandem Elliptical Cam Technique'. The original profile once filtered, gives a different effective profile.

4.2.2 Low-Pass Filtering

The profile once filtered using the 'Tandem Elliptical Cam Technique' still has discontinuities due to the underlying road profile. These can cause spikes in the vertical velocity input to the quarter-car model.

A first order Butterworth filter was used as a low-pass filter to reduce these discontinuities. The break frequency was chosen to be 150 Hz, since the dynamics we were interested in fall within this frequency.

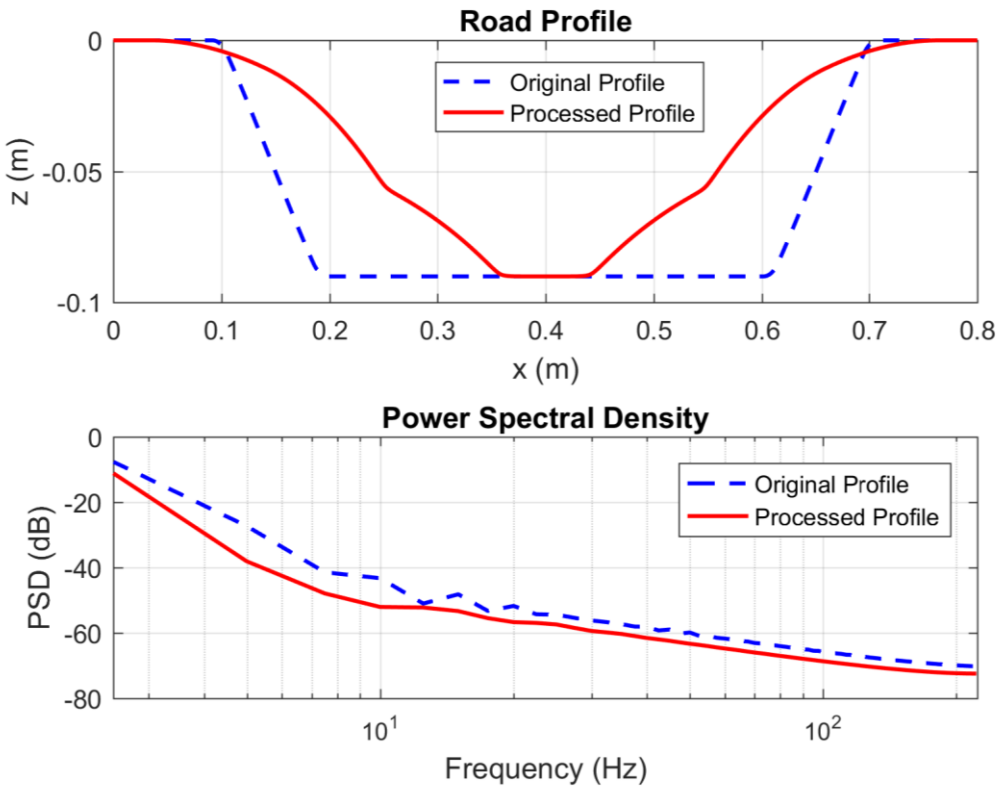

Figure 4.14: Processing of road profiles

Figure 4.14 shows the result of processing a road profile with both, the 'Tandem Elliptical Cam Technique' and adding a low-pass filter to eliminate discontinuities. A smoother profile is obtained.

4.2.3 Obtaining Vertical Velocity Profile

The obtained profile gives us the vertical displacement of the wheel as a function of horizontal travel. However, the required input for the developed quarter-car model is a vertical velocity profile as a function of time.

For a given vehicle velocity, the profile can be converted to vertical displacement as a function of time. The vertical displacement was then differentiated with respect to time to obtain a vertical velocity profile as a function of time. This serves as the unilateral boundary condition for the quarter-car model.

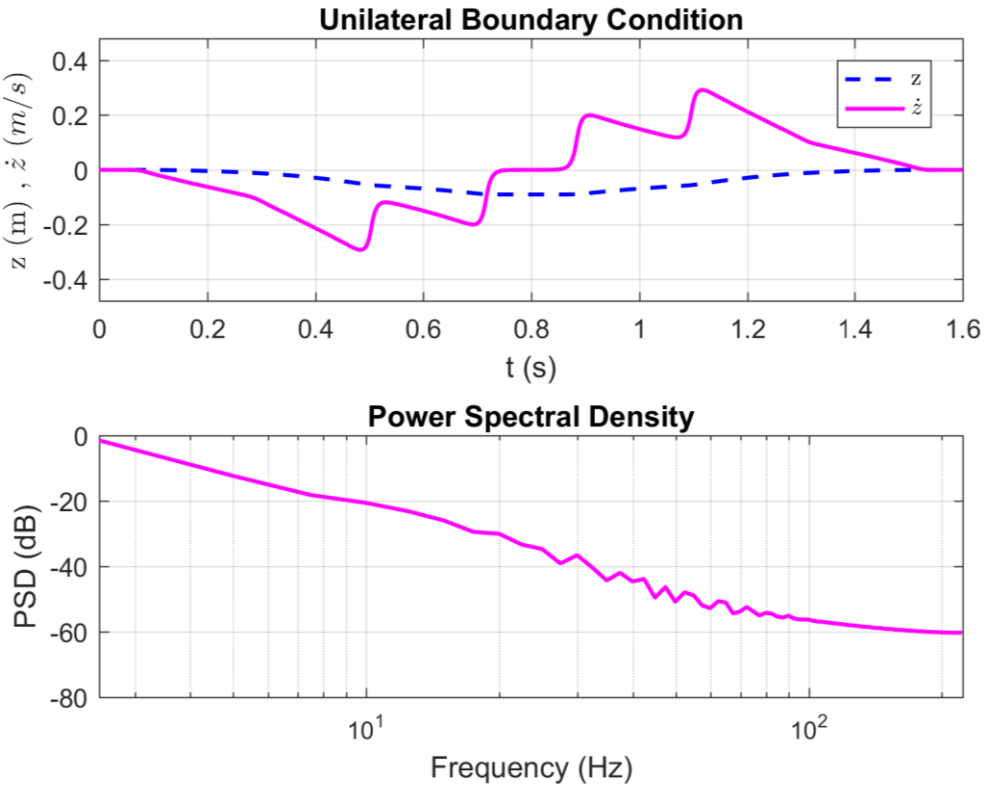

Figure 4.15: Unilateral boundary condition

Figure 4.15 shows the unilateral boundary condition for the quarter-car model obtained using this method. For different vehicle velocities, the vertical displacement profile results in different vertical velocity profiles.

5 Optimized Control Force Estimation

Given a dynamic vehicle model, single-event road obstacle profile the aim of this research is to determine the ideal control force profile to achieve the control objective. It is possible to find this control force profile using offline optimization. Adaptive filtering is perfectly suited to this task.

Adaptive filtering makes use of a cost function for optimization. The results of optimization will depend on the chosen cost function for minimization. In the current problem of active suspensions, adaptive filtering can be used to optimize either ride comfort, handling, or minimize the rattle space. In the work presented here, ride comfort was chosen as the objective. By changing the cost function, other objectives can also be achieved.

The performance indices relating ride comfort and handling are often measured by the root-mean-square (RMS) values of sprung mass acceleration and tire deflection respectively [28]. Therefore, the expected value of squared sprung mass acceleration was chosen as the main parameter for the cost function given by (5.1) which needs to be minimized.

$$J(F_c) = \left(\frac{1}{T}\right) \int_{event} a_s^2(t)dt \tag{5.1}$$

The method used for adaptive filtering is the Filtered-X-LMS algorithm, which is an extension of the LMS optimization method.

5.1 LMS Optimization

The LMS optimization method [20] is used to obtain an ideal filter that can minimize the error between its output signal and a desired signal.

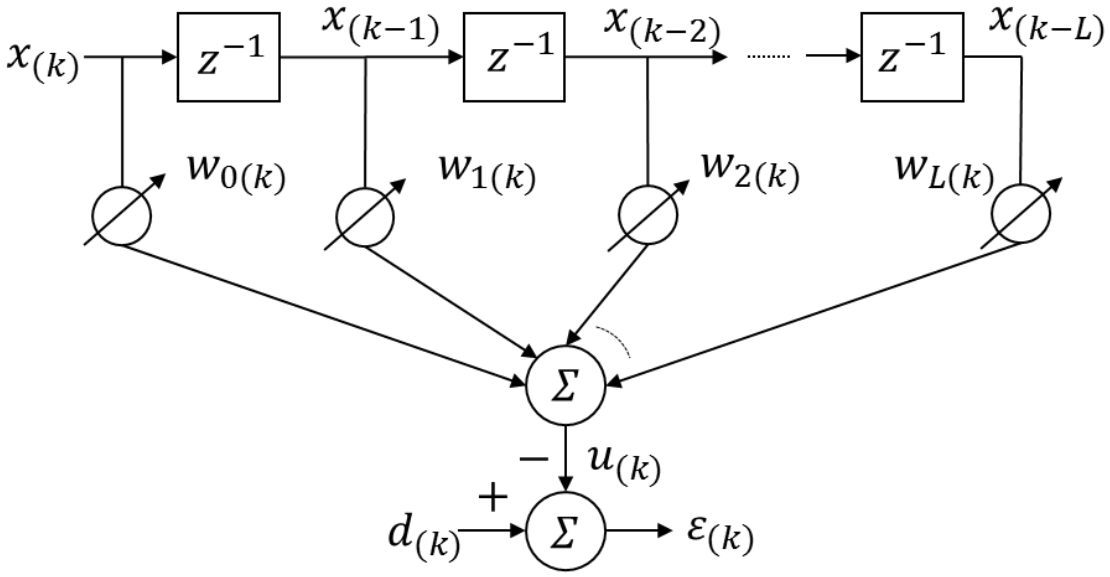

Figure 5.1: Adaptive linear combiner

Figure 5.1 shows a schematic diagram of an adaptive linear combiner. It is a time-varying, non-recursive digital filter. There is an input signal vector $X_{(k)}$ with elements $x_{(k-L)}$ … $x_{(k-1)}$ up to $x_{(k)}$ and a corresponding set of adjustable weights $W_{(k)}$ with elements $w_{o(k)}$, $w_{1(k)}$, … $w_{L(k)}$, a summing unit, and a single output signal $u_{(k)}$, where (k) represent the k[th] time index and L is the number of weights.

$$u_{(k)} = \sum_{l=0}^{L} w_{l(k)} x_{(k-l)} \tag{5.2}$$

For a fixed setting of the weights, the output is a linear combination of the inputs (5.2). The output signal $u_{(k)}$ is subtracted from the desired signal $d_{(k)}$ to produce the error signal $\varepsilon_{(k)}$. The adaptation process is designed to reduce this error.

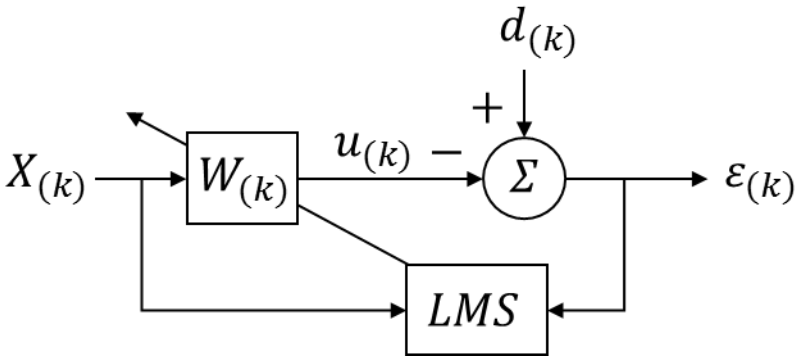

Figure 5.2: LMS algorithm

Using the LMS algorithm shown in Figure 5.2, the weights can be adapted. The vector of weights for the next time index $W_{(k+1)}$ is obtained using a gradient descent method and is given by equation (5.3), where μ is the gain constant that regulates the speed and stability of adaptation.

$$W_{(k+1)} = W_{(k)} + \mu\varepsilon_{(k)}X_{(k)} \tag{5.3}$$

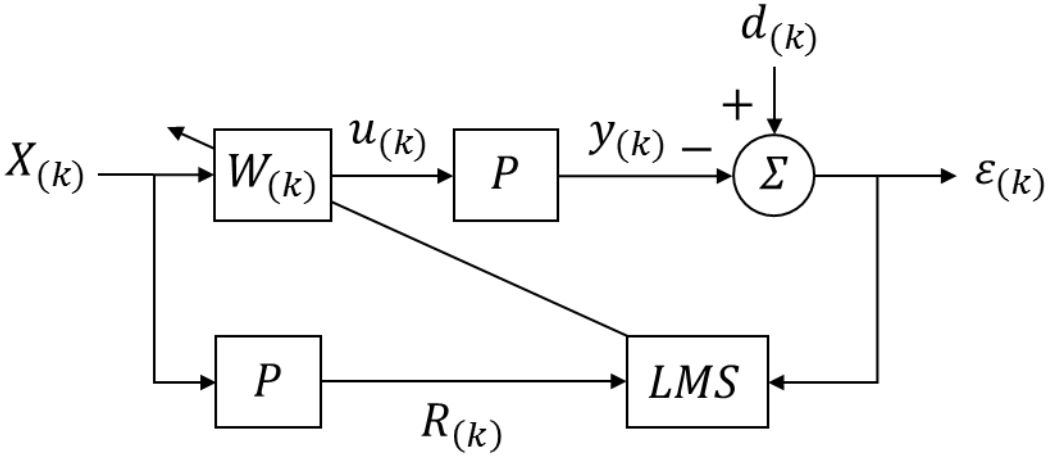

Figure 5.3: Filtered-X LMS Algorithm

Figure 5.3 shows the Filtered-X LMS or Fx-LMS algorithm which is an extension of the basic LMS algorithm. It is required when a dynamic system P exists after the adaptive filter. In this algorithm, the input $X_{(k)}$ is filtered by the plant P and this is used by the

LMS algorithm. The vector of weights for the next time index $W_{(k+1)}$ is obtained using a gradient descent method and is given by equation (5.4).

$$W_{(k+1)} = W_{(k)} + \mu\varepsilon_{(k)}R_{(k)} \tag{5.5}$$

While the LMS algorithm is used for system modeling, the Fx-LMS algorithm works well for inverse filtering. The Fx-LMS algorithm converges to de-correlate ε from d .

5.1.1 Iterative LMS Adaptation

Since the focus was on single-event obstacles, which are not persistent, an iterative batch modification was required. When the Fx-LMS algorithm in Figure 5.3 is used on a batch of input X , an optimized vector of weights W is obtained. The algorithm can then be used again on the same batch of input, but this time, the W vector from the previous iteration can be used as an initial condition. In this way, the vector of weights W is optimized further in each iteration. This will be referred to as Iterative LMS adaptation.

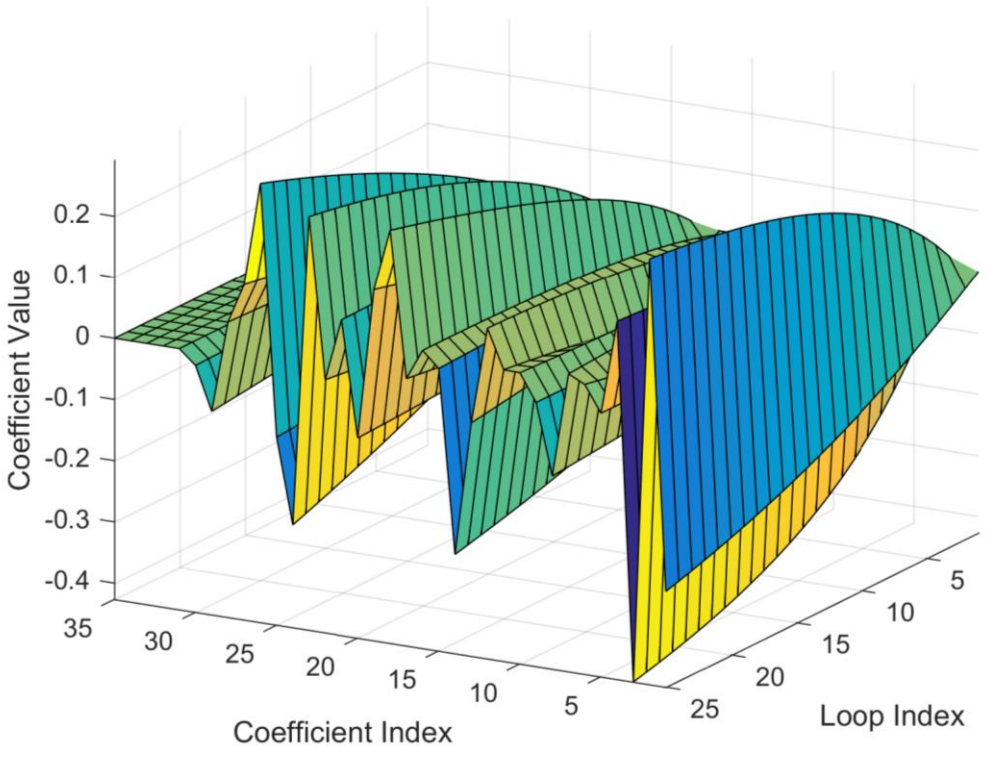

Figure 5.4: Iterative LMS Adaptation of filter coefficients

Figure 5.4 shows how the filter W gets optimized over each iteration. In this example, W was chosen to have 35 coefficients and 25 iterations were used to obtain the final filter. This illustrates how the Iterative LMS Adaptation works offline on the same batch of input multiple times until the final filter W is obtained. This also enables a way to directly evaluate convergence.

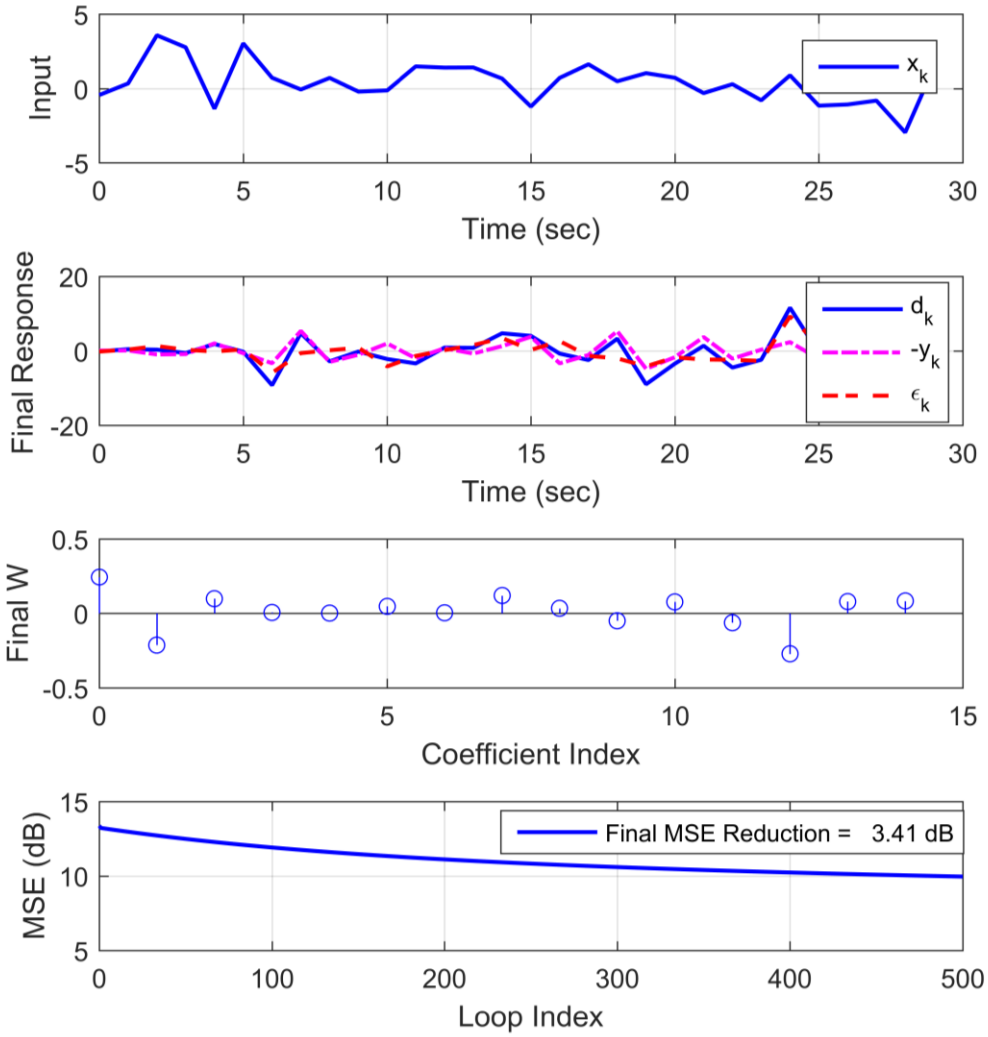

Figure 5.5: Iterative LMS Adaptation – poor performance

Figure 5.5 shows the Iterative LMS Adaptation for a randomly generated SISO plant model P, a random input x_k and a random desired response d_k. It is seen that after running the algorithm for 500 iterations, the mean square error between the desired response d_k and output y_k reduces by 3.41 dB, which is not acceptable.

The performance of the algorithm depends on two very important parameters, the step size μ and the number of filter coefficients in W. We can use these as knobs to adjust the performance.

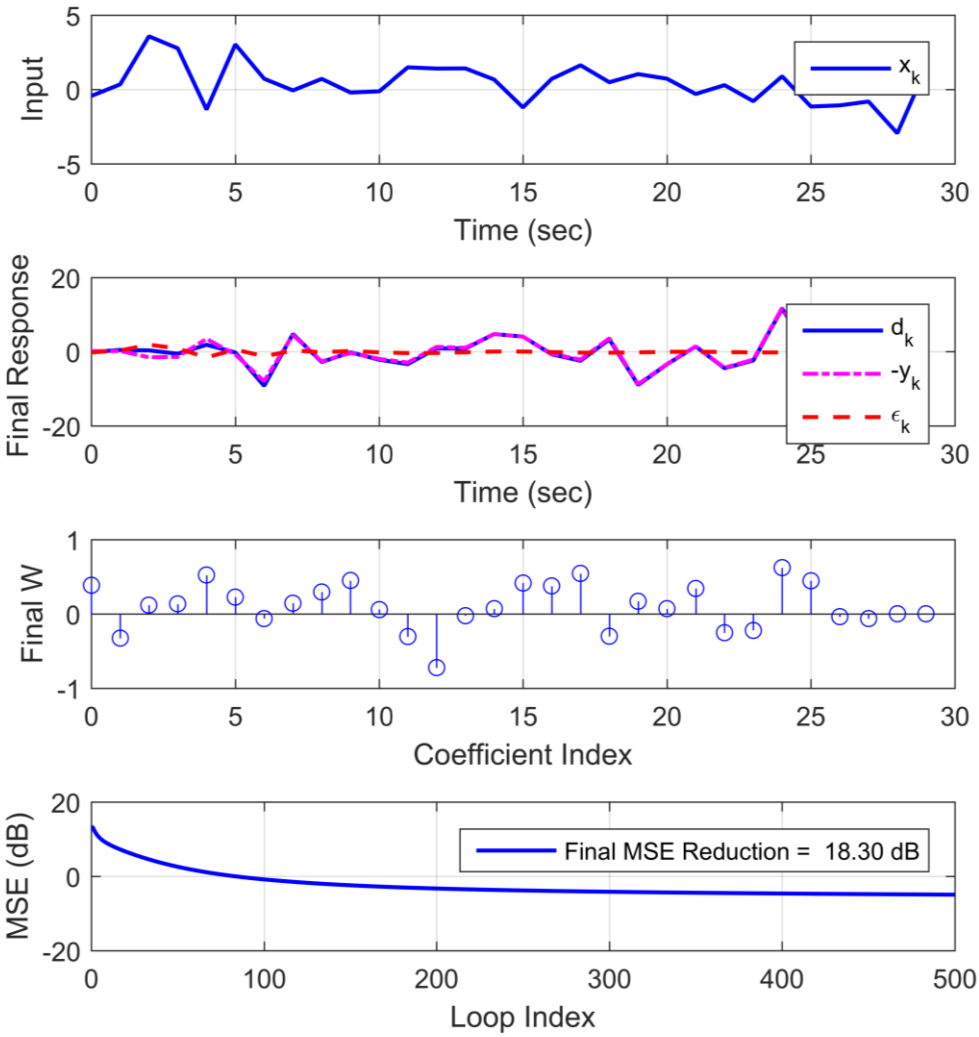

Figure 5.6: Iterative LMS Adaptation - good performance

Figure 5.6 shows the results of changing the step size μ and the number of filter coefficients in W. It is seen that over the same number of iterations (500), a much better performance is obtained with over 18 dB reduction of error. The filter has converged. There is no simple formula to determine the best step size and number of coefficients. They depend on the dynamics of the problem and have to determined by trial and error.

Figure 3.3 shows the state space model of the quarter car. The paths between the road input $\dot{z}_r$, the control effort F_c and the sprung mass acceleration a_s are the paths of interest.

The Iterative LMS Adaptation is used to develop a controller that applies the required control effort that can de-correlate the sprung mass acceleration from the road input, assuming an actuator with unlimited authority.

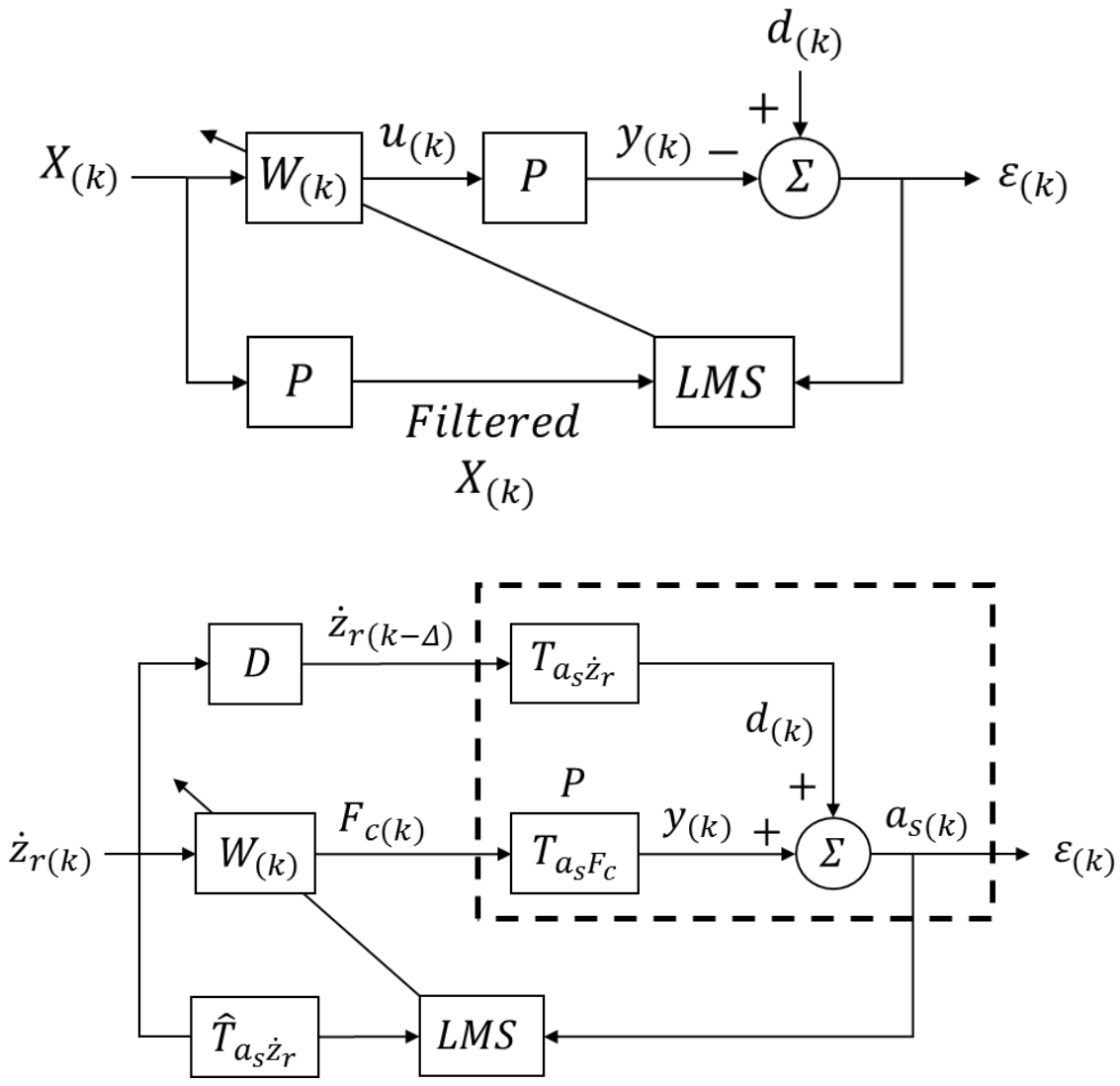

Figure 5.7: Fx-LMS algorithm applied to quarter-car model

Figure 5.7 shows the application of the iterative LMS Adaptation to the quarter-car model where the original form of the Fx-LMS algorithm is shown for comparison. The road input

is $\dot{z}_{r(k)}$ and is delayed by Δ samples to give $\dot{z}_{r(k-\Delta)}$ which is applied to the quarter-car. This mean that $\dot{z}_{r(k)}$ is effectively preview information for LMS adaptation. Using this preview information, the adaptation is performed to optimize the adaptive filter coefficients in $W_{(k)}$ which produces the control effort $F_{c(k)}$ for the plant P. The resulting sprung mass acceleration $a_{s(k)}$ due to the road disturbance $d_{(k)}$ and control effort $F_{c(k)}$ is the error $\varepsilon_{(k)}$, which will get de-correlated from the input after convergence. The simplified case is assumed in which perfect knowledge of the system models and measured road input are available.

The resulting control effort can be analyzed to determine the peak force and bandwidth required to overcome the specific road obstacle profile.

5.2 FIR Filter Model

The state space model equations (3.5) are in continuous time and not suitable for Iterative LMS Adaptation. The Fx-LMS algorithm is designed to work only with FIR filter models. Finite Impulse Response (FIR) filters were chosen for discretizing the system.

FIR filters for each path in Figure 3.3 that represent the transfer functions for the system were used to create the discrete model. An impulse response can be generated for each path and this creates the FIR filter for the path.

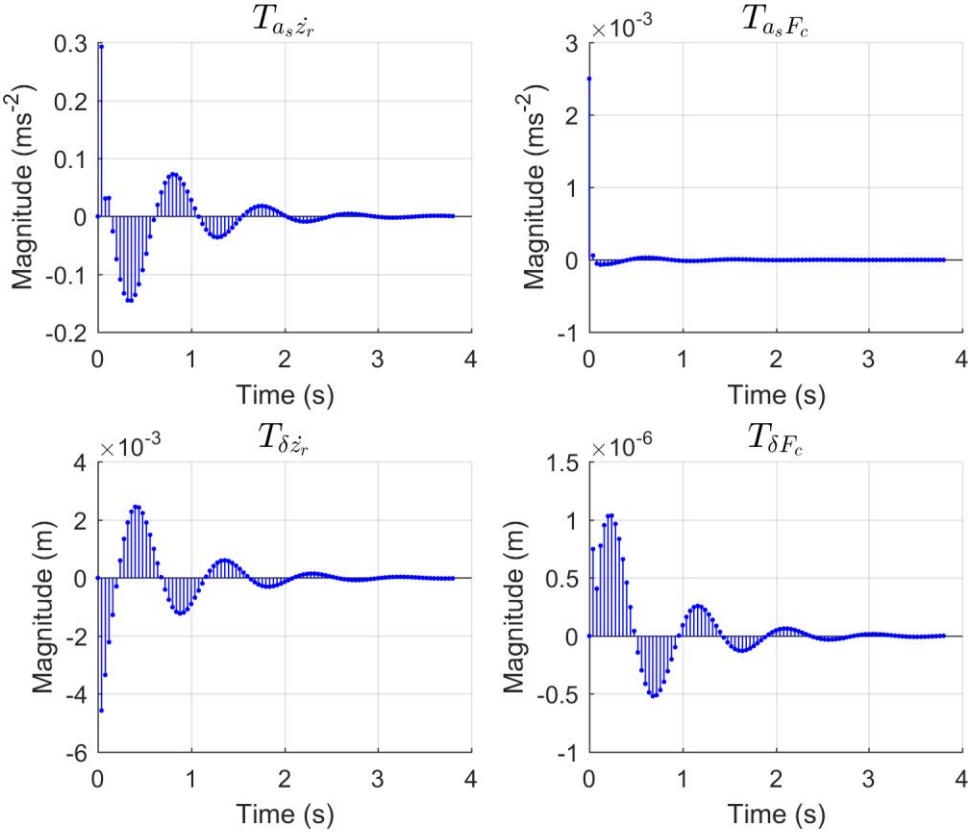

Figure 5.8: FIR filters for transfer function paths

Figure 5.8 shows the FIR filters that represent the quarter car model. There are two inputs, namely the vertical velocity due to the road profile $\dot{z}_r$ and the control effort F_c. There are also two outputs namely the sprung mass acceleration a_s and suspension deflection δ. Therefore there are four possible paths from inputs to outputs.

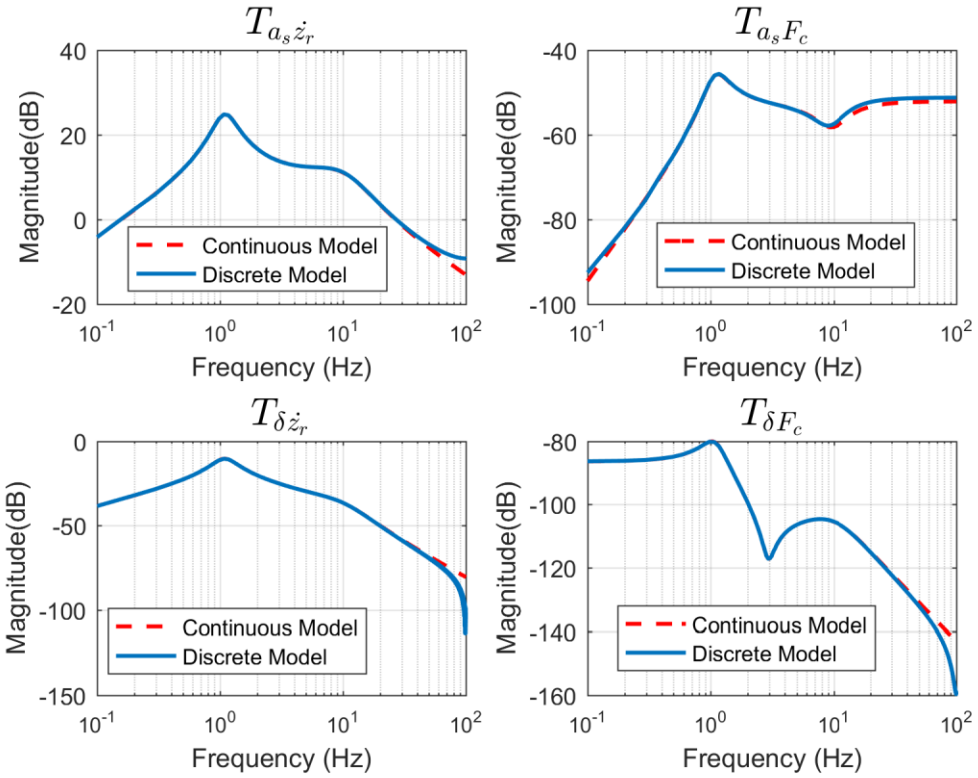

Figure 5.9: Transfer functions for quarter-car model

Figure 5.9 shows the transfer function for each path. It is seen that the FIR filter discrete model is a very good approximation of the continuous model.

5.2.1 Model Regeneration

The simulations were performed for different vehicle velocities. When the vehicle velocity is increased, the input discrete road excitation takes a much shorter time as shown in Figure 5.10.

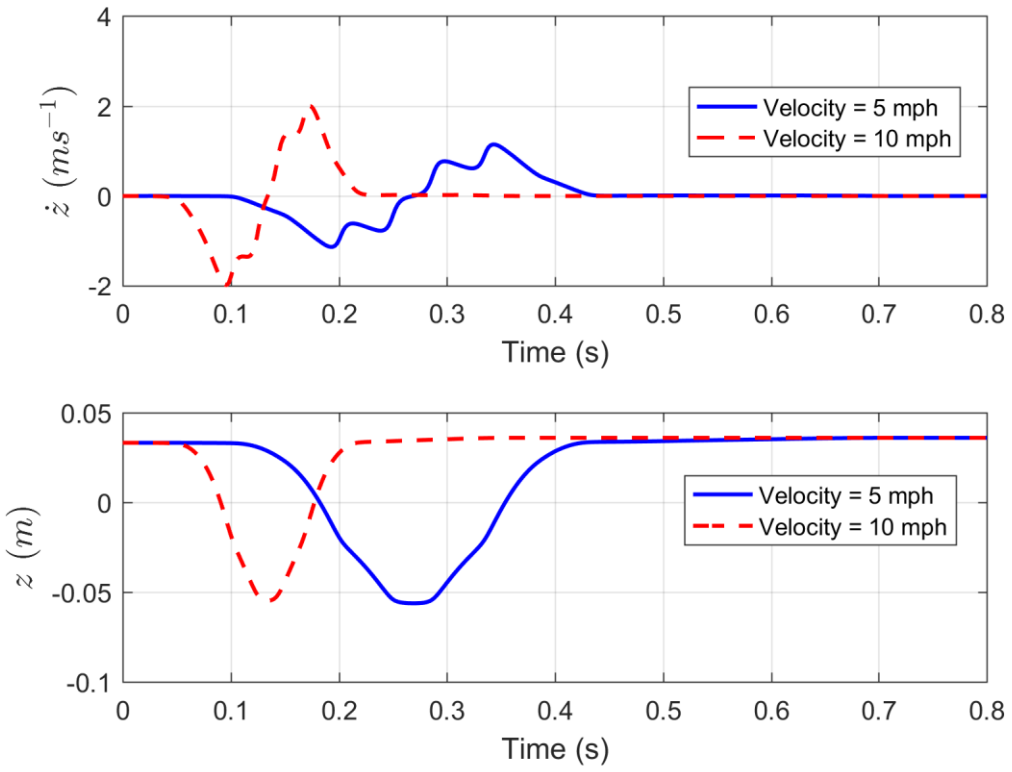

Figure 5.10: Velocity input *comparison*

Therefore, a higher sample rate had to be used for higher velocities so that the discretized vertical displacement accurately represents the original road profile input. The FIR filters are only suitable for use at the sample rate at which they are generated. For this reason, each time the vehicle velocity was changed, the FIR filters were re-generated for the new sample rate.

6 Results

A case study was conducted using Iterative LMS adaptation together with the discrete-time quarter-car model to obtain the required control effort for different road obstacle profiles.

The continuous model was first created using the selected vehicle parameters.

A road profile was then selected for the case study. This road profile was sampled at a chosen sampling rate which was low enough to not be too processor intensive and yet high enough to accurately represent the geometry of the profile. A randomly generated road profile based on ISO standards was added to the profile to better represent road conditions.

It was then processed with the ‘Tandem Elliptical Cam Technique’ to account for the interaction of the tire with the profile and then filtered using a Butterworth filter to get rid of discontinuities. This profile was then differentiated to obtain a vertical velocity profile that served as input to the quarter-car model.

Having selected a sampling rate for the profile, the continuous quarter-car model was used to obtain a discrete model at this sampling rate with FIR filters that had enough coefficients to accurately represent the quarter-car dynamics.

Iterative LMS adaptation was used to obtain the ideal control effort to de-correlate the system response from the road obstacle input.

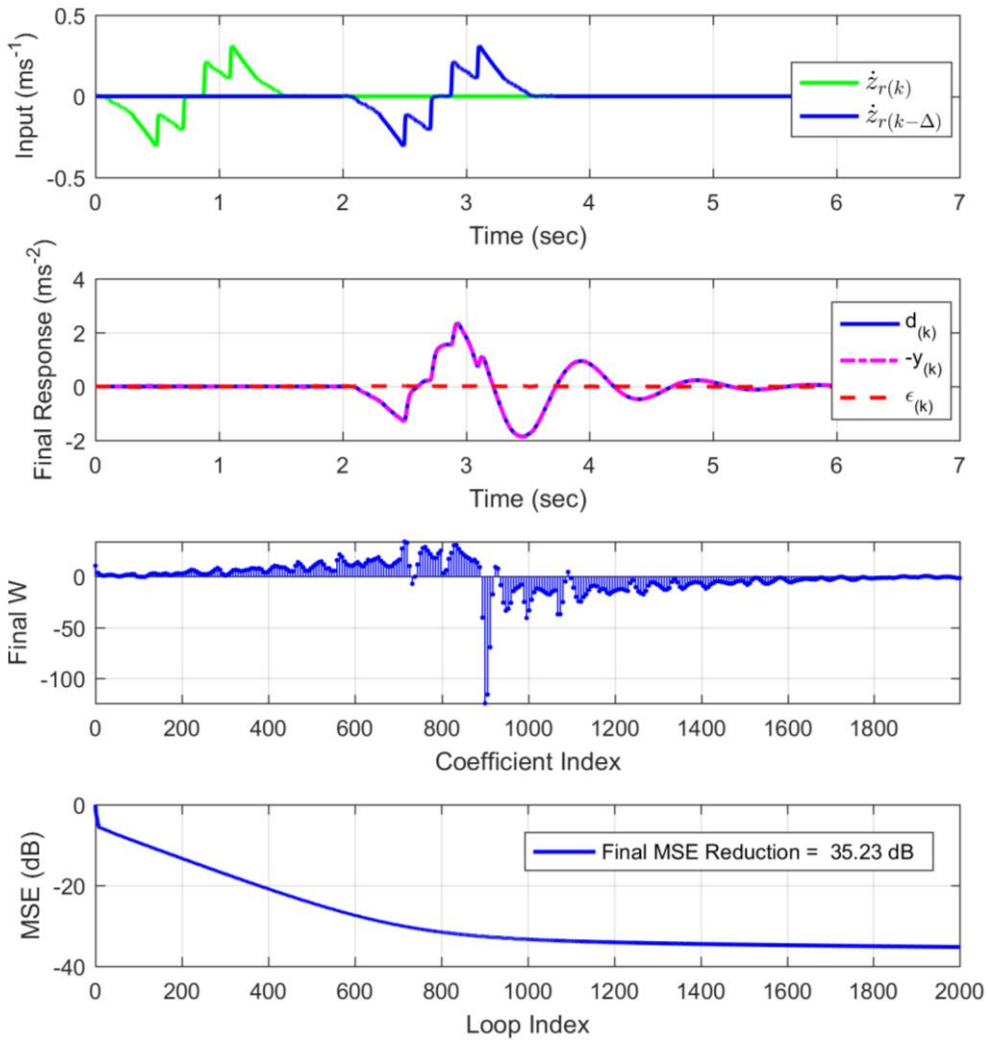

Figure 6.1: Iterative LMS Adaptation applied to quarter-car

Figure 6.1 shows the development of a filter for a quarter-car using Iterative LMS Adaptation. The input to the model is shown in the first plot. It was a pothole at a low velocity represented by the blue curve $\dot{z}_{r(k-\Delta)}$. Preview information for LMS adaptation is represented by the green curve $\dot{z}_{r(k)}$. The output due to the road obstacle profile is d, while the output due to the control effort applied to the plant is y. The difference between them is the resulting sprung mass acceleration a_s, or the error ε which needs to be reduced. The mean square error (MSE) was compared between the sprung mass acceleration with control and without control. It is directly related to the root-mean-square value of sprung

mass acceleration, which is the main performance index of a suspension. It was seen that after 2000 iterations, the final filter W was obtained and the mean square error of the sprung mass acceleration reduced by over 35 dB. This high reduction was obtained by suitably choosing the step size μ and number of coefficients in W.

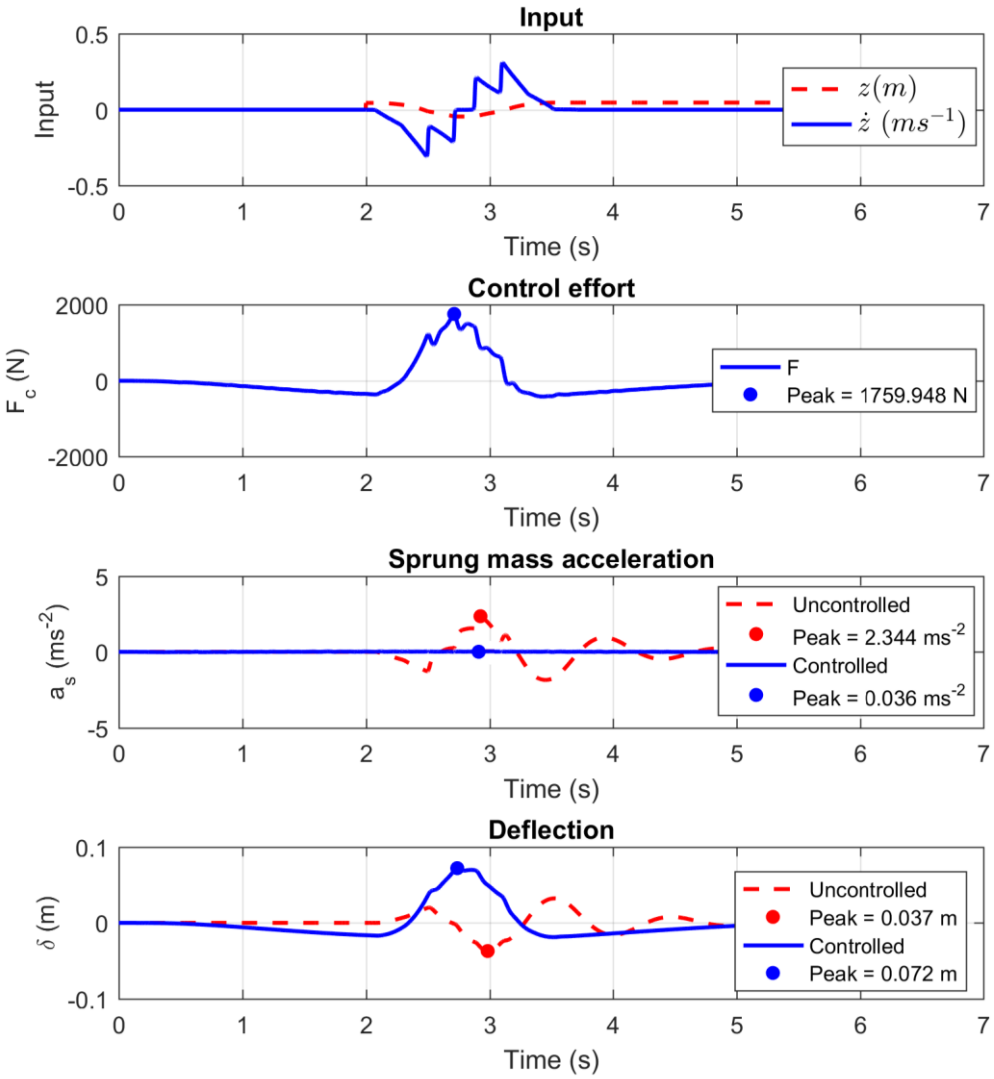

Figure 6.2: Controlled quarter-car model response

Figure 6.2 shows the time-series plots for the control of the quarter-car model using the obtained filter. There were certain key performance metrics for each simulation.

- Peak acceleration
- Peak Control Force

- Bandwidth
- Peak Deflection

The sprung mass acceleration a_s was drastically reduced and the peak acceleration can be obtained from the plot of sprung mass acceleration in Figure 6.2 . The plot of control effort F_c is shown and is used to obtain the peak force. The suspension deflection δ is also obtained and can be used if the control goal changes from ride comfort. The bandwidth can be obtained from the PSD of the control force profile.

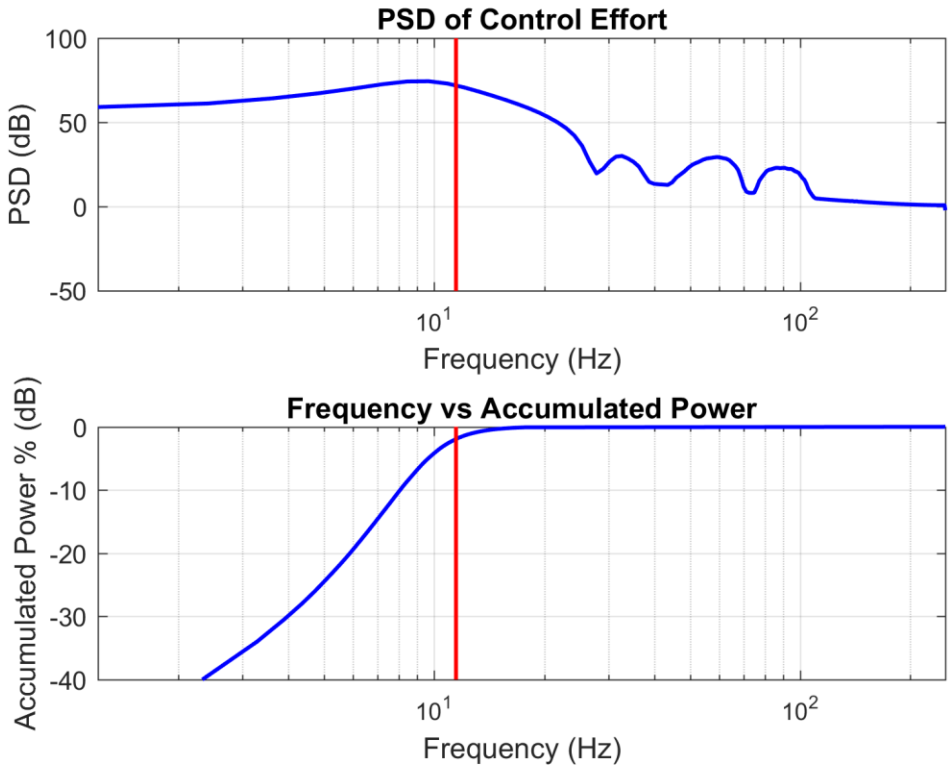

Figure 6.3: 80% Power Bandwidth

Figure 6.3 shows the PSD of the control effort. The bandwidth is not evident from the plot since there is no easily determined -3dB point. Instead, a plot of frequency versus the percentage of total power is used to find the frequency within which 80% of the total power is present. This is approximately equivalent to the -3dB frequency of a 2nd order low pass filter and is a good metric for the bandwidth.

$$P = \left\{ f(\mathrm{J}) : \frac{\sum_{i=1}^{J} PSD(\mathrm{i})}{\sum_{i=1}^{N} PSD(\mathrm{i})} = 0.8, J \in \mathbb{N} \right\} \tag{6.1}$$

This will be referred to as the 80% Power Bandwidth and is given by equation (6.1) where $f(J)$ is the frequency at frequency bin J and N is the total number of frequency bins for the PSD. We see that for the chosen input, more than 80 percent of the total power is below 11 Hz represented by the red line.

The simulation was run for each unique road input with multiple combinations of vehicle velocities and preview distances as shown in Table 5. Nine hundred simulations were performed in total.

Table 5: Simulation Conditions

Road Profile
Speed Hump Watts Profile
Speed Hump Seminole Profile
Curb A
Curb B
Curb C
Curb D
Curb E
Curb F
Curb G
Uneven Road A
Uneven Road B
Uneven Road C
Pothole P1
Pothole P6
Pothole P9

Preview Distance (m)
0
0.5
1
1.5
2

Vehicle Velocity (mph)
5
10
15
20
25
30
35
40
50
60
70
80

The simulations were run for realistic preview information ranging from no look-ahead preview, to look ahead preview of two meters ahead. It should be noted that although look ahead preview is practically realized as a distance, it is helpful to the algorithm because of the additional time steps available for adaptation. In [12] it was found that preview times of even 0.2 s were valuable. However, even the maximum preview distance of two meters translates to only 0.4474 s at a low velocity of 10 mph and 0.056 s at a high velocity of 80

mph. Therefore, at high velocities, the look ahead preview has a negligible effect. It was also found in [16] that preview information results in no improvement past a certain time, approximately 0.5 s. This maximizes the use of preview at low vehicle velocities for the work presented in this thesis at a preview distance of 2 m.

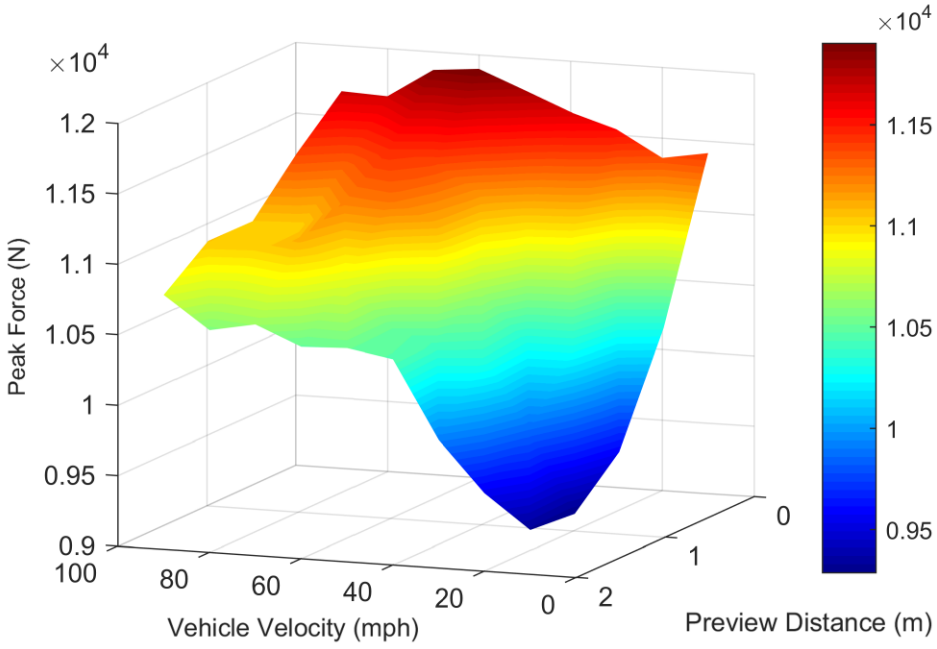

Figure 6.4: Peak force surface for non-converged filter W

It was found that, when a non-converged filter W was used, the performance of the control effort was poor. For this undesirable condition, preview distance had a high impact on the results of the simulation since it was used to improve the performance. This is shown in Figure 6.4.

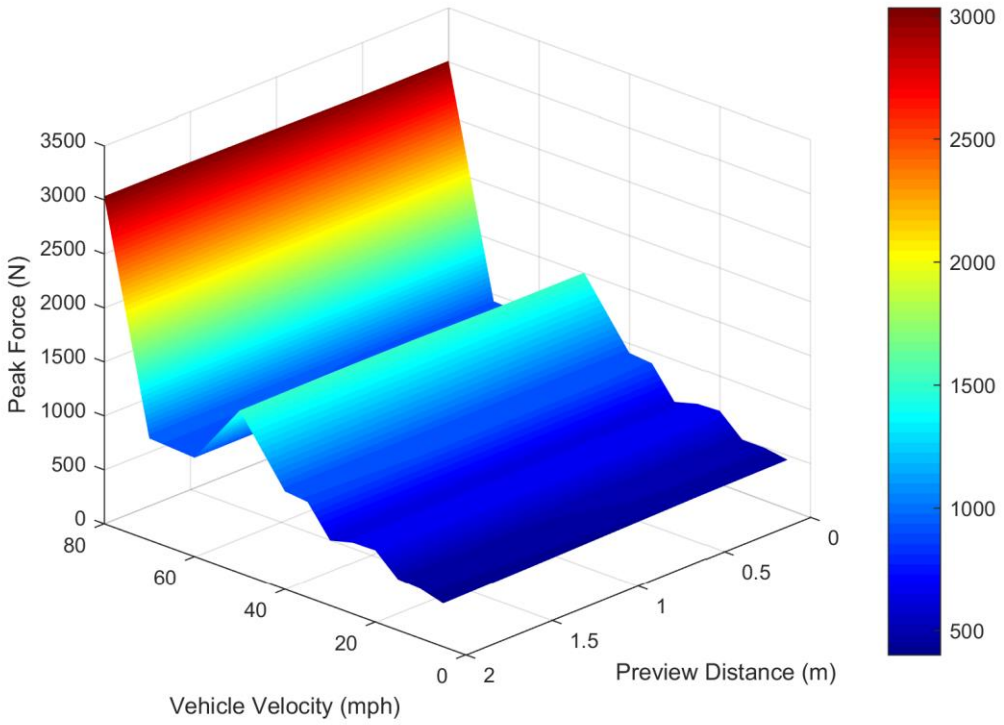

Figure 6.5: Peak force surface for converged filter W

Figure 3.1 shows the results of simulation when a properly converged filter W was used. The preview distance did not have much of an effect.

The results are presented for four of the types of profiles of importance. The complete set of results are in the Appendix.

6.1.1 Case study results: Curb A

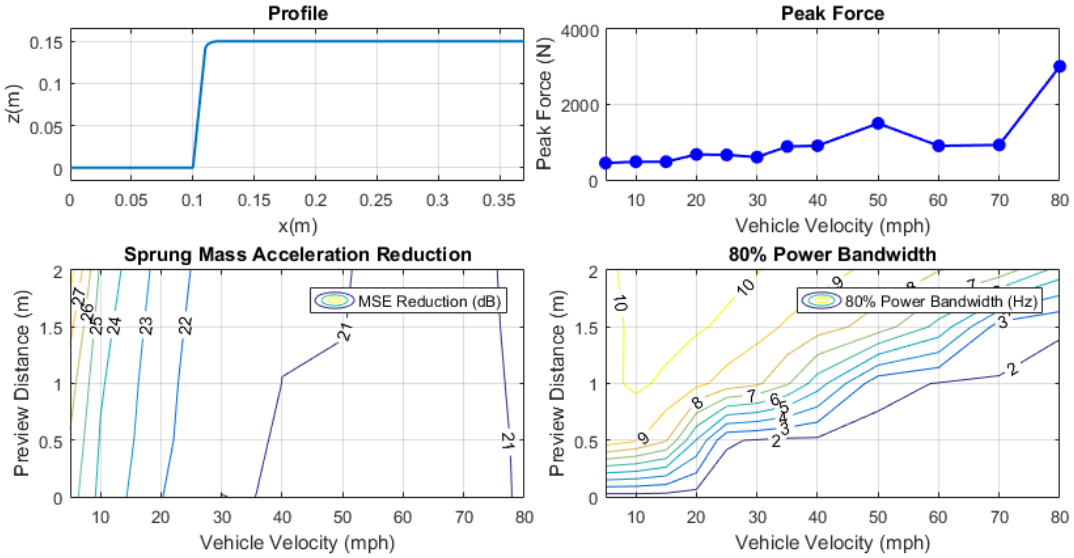

Figure 6.6: Results for Curb A

The simulations were performed for the 'Curb A' profile. Figure 6.6 shows the peak force and bandwidth for different vehicle velocities and preview distances. Peak force requirement generally increases as the vehicle velocity increases. There is a minor effect of preview distance on the sprung mass acceleration reduction. At higher velocity, the sprung mass acceleration reduction decreases. However, it is always over 20 dB which means that the ideal control-force profile performs very well. Higher bandwidth is required at lower velocities and high preview distances.

6.1.2 Case study results: Pothole P1

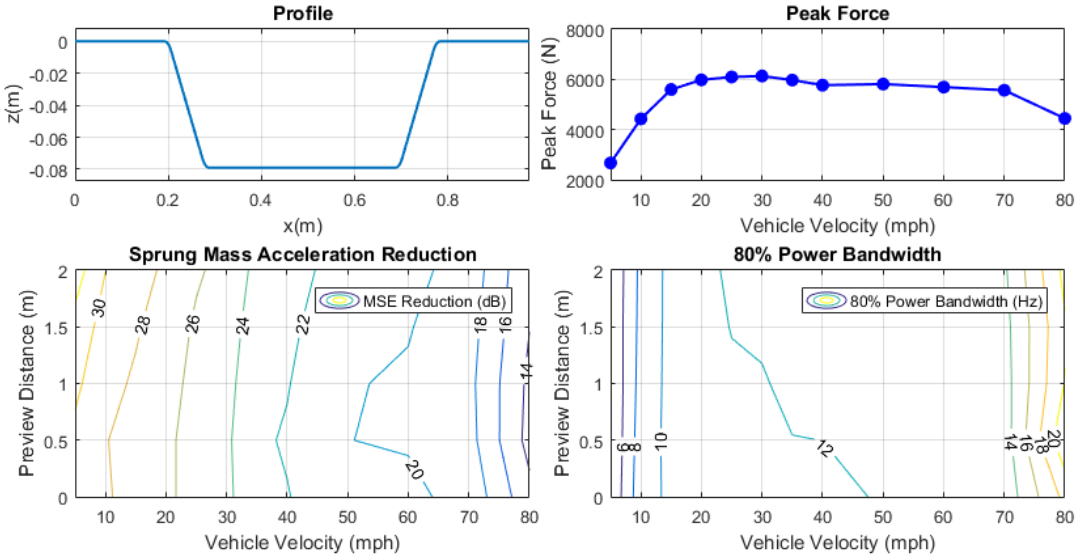

Figure 6.7: Results for Pothole P1

The simulations were performed for 'Pothole P1'. Figure 6.7 shows the peak force and bandwidth for different vehicle velocities and preview distances. For the pothole, the peak force increases initially and reduces at higher velocities. The preview distance does not have much effect on the sprung mass acceleration reduction or bandwidth requirements. At higher velocities, the sprung mass acceleration reduction reduces. The performance of the ideal control-force profile is always good, with over 14 dB of sprung mass acceleration reduction in all cases.

6.1.3 Case study results: Speed Hump Watts Profile

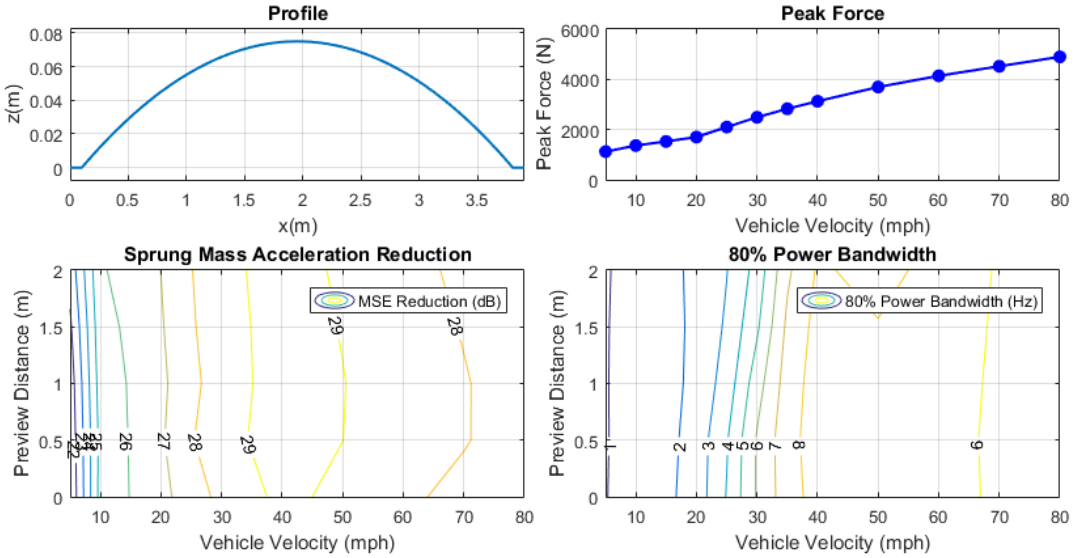

Figure 6.8: Results for Speed Hump Watts Profile

The simulations were performed for a speed hump with a Watts Profile. Figure 6.8 shows the peak force and bandwidth for different vehicle velocities and preview distances. For the speed hump, the peak force increases as the vehicle velocity increases. The preview distance does not have much effect on the sprung mass acceleration reduction. At higher velocities, the sprung mass acceleration reduction reduces. The performance of the ideal control force is very good with over 28 dB of reduction in all cases. The preview distance does not have much of an effect on the bandwidth requirements.

6.1.4 Case study results: Uneven Road A

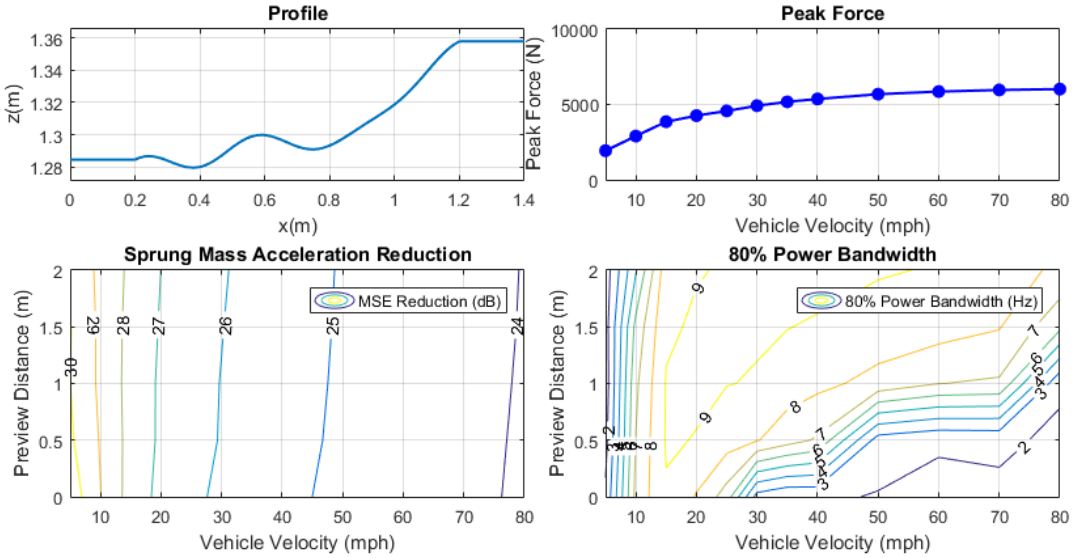

Figure 6.9: Results for Uneven Road A

The simulations were performed for 'Uneven Road A', which is of very poor quality (class F). Figure 6.7 shows the peak force and bandwidth for different vehicle velocities and preview distances. For the uneven road profile, the peak force increases as the vehicle velocity increases. The preview distance does not have much effect on the sprung mass acceleration reduction. At higher velocities, the sprung mass acceleration reduction reduces. The performance of the ideal control force is very good with over 24 dB of reduction in all cases. Higher bandwidth is required at certain velocities and high preview distances. This suggests that the characteristics of the obstacle influence the required bandwidth more at certain vehicle velocities.

7 Conclusions

The peak force requirement depends on the vehicle velocity and profile characteristics or excitation. The bandwidth requirements are affected by the velocity of the vehicle and look-ahead preview.

This research showed that vehicle velocity has a much greater effect on peak force and bandwidth than look-ahead preview, but the trend depends on the profile.

For this study, the effects of look-ahead preview appears to only depend on convergence and numerical issues.

The developed processing method using the 'Tandem Elliptical Cam Technique' and filtering were easily applied to all types of road profiles and gave results similar to those applied in practical testing from literature [18].

The ideal control force profile obtained with the help of Iterative LMS adaptation performed very well regardless of the road obstacle profile and velocity of the vehicle in a consistent manner, with over 18 dB of reduction in sprung mass acceleration in all cases.

7.1 Contributions

The iterative LMS adaptation method was developed to determine the ideal control effort which was shown to be very effective at de-correlating the response of a quarter-car from a known single-event excitation.

A discrete quarter-car model well suited to the iterative LMS adaptation method was developed.

A database of twelve single-event road obstacle profiles including road unevenness was created based on standards and existing literature.

The 'Tandem Elliptical Cam Technique' was used to account for the enveloping effect of tires and represent road-tire interaction more accurately.

Case studies were performed by simulating the response of the developed quarter-car model using different road obstacles. The results were used to determine the peak force

and bandwidth of the required actuation. The developed method is generalized and allows for modification in the system model and boundary conditions.

7.2 Future Work

The quarter-car model can be extended to a full-vehicle model to allow for more realistic simulations of vehicles due to rolling and pitching and also more actuators for active suspension control. Iterative LMS Adaptation can also be applied to higher degree of freedom models.

Along with increasing the variety of road obstacles, non-unilateral boundary conditions such as soft soil or road breakaway could be developed to improve the simulation of road-tire interaction.

The results of simulation can be used to design actuators well suited to the control of active suspensions. The Quarter-car testing rig developed by Justin Langdon [29] can be used for practical testing of a custom built actuator with the control effort obtained through Iterative LMS Adaptation.

8 References

1. Tseng, H.E. and D. Hrovat, *State of the art survey: active and semi-active suspension control.* Vehicle System Dynamics, 2015. **53**(7): p. 1034-1062.
2. Sharp, R.S. and D.A. Crolla, *Road Vehicle Suspension System Design - a review.* Vehicle System Dynamics, 1987. **16**(3): p. 167-192.
3. Gysen, B.L., et al., *Active electromagnetic suspension system for improved vehicle dynamics.* IEEE Transactions on Vehicular Technology, 2010. **59**(3): p. 1156-1163.
4. Weeks, D., et al., *The design of an electromagnetic linear actuator for an active suspension*. 1999, SAE Technical Paper.
5. Iijima, T., et al., *Development of a hydraulic active suspension*. 1993, SAE Technical Paper.
6. Ghazaly, N.M. and A.O. Moaaz, *The Future Development and Analysis of Vehicle Active Suspension System.* IOSR Journal of Mechanical and Civil Engineering, 2014. **11**(5): p. 19-25.
7. Thompson, A., *An active suspension with optimal linear state feedback.* Vehicle system dynamics, 1976. **5**(4): p. 187-203.
8. Ting, C.-S., T.-H.S. Li, and F.-C. Kung, *Design of fuzzy controller for active suspension system.* Mechatronics, 1995. **5**(4): p. 365-383.
9. Nguyen, T.T., et al. *A hybrid control of active suspension system using H∞ and nonlinear adaptive controls*. in *Industrial Electronics, 2001. Proceedings. ISIE 2001. IEEE International Symposium on*. 2001. IEEE.
10. Munari, L.A., et al., *Retrieving Road Surface Profiles from PSDs for Ride Simulation of Vehicles*. 2012, SAE Technical Paper.
11. Dodds, C. and J. Robson, *The description of road surface roughness.* Journal of sound and vibration, 1973. **31**(2): p. 175-183.
12. Bender, E.K., *Optimum Linear Preview Control With Application to Vehicle Suspension.* Journal of Basic Engineering, 1968. **90**(2): p. 213-221.
13. Tomizuka, M., *"Optimum Linear Preview Control With Application to Vehicle Suspension"—Revisited.* Journal of Dynamic Systems, Measurement, and Control, 1976. **98**(3): p. 309-315.
14. Louam, N., D. Wilson, and R. Sharp, *Optimal control of a vehicle suspension incorporating the time delay between front and rear wheel inputs.* Vehicle system dynamics, 1988. **17**(6): p. 317-336.
15. Adibi Asl, H. and G. Rideout. *Using lead vehicle response to generate preview functions for active suspension of convoy vehicles*. in *American Control Conference (ACC), 2010*. 2010.
16. Hać, A., *Optimal linear preview control of active vehicle suspension.* Vehicle system dynamics, 1992. **21**(1): p. 167-195.
17. Agostinacchio, M., D. Ciampa, and S. Olita, *The vibrations induced by surface irregularities in road pavements - a Matlab approach.* European Transport Research Review, 2014. **6**(3): p. 267-275.

18. Schmeitz, A.J.C., *A Semi-Empirical Three-Dimensional Model of the Pneumatic Tyre Rolling over Arbitrarily Uneven Road Surfaces*. 2004, Delft University of Technology: Institutional Repository. p. 320.
19. Pacejka, H., *Tire and Vehicle Dynamics*. 2 ed. 2006: Butterworth-Heinemann. 672.
20. Bernard Widrow, S.D.S., *Adaptive Signal Processing*. 1985: Prentice Hall. 475.
21. Song, X., et al., *An Adaptive Semiactive Control Algorithm for Magnetorheological Suspension Systems.* Journal of Vibration and Acoustics, 2005. **127**(5): p. 493-502.
22. Plaxico, C.A., et al., *Recommended Guidelines for Curb and Curb-Barrier Installations*. 2005: United States. p. 112p.
23. Parkhill, M., R. Sooklall, and G. Bahar. *Updated guidelines for the design and application of speed humps*. in *Institute of Transportation Engineers Annual Meeting and Exhibit 2007, August 5, 2007 - August 8, 2007*. 2007. Pittsburgh, PA, United states: Institute of Transporation Engineers.
24. Weber, P.A. and J.P. Braaksma, *Towards a North American geometric design standard for speed humps.* ITE Journal (Institute of Transportation Engineers), 2000. **70**(1): p. 30-34.
25. Miller, J.S. and W.Y. Bellinger, *Distress identification manual for the long-term pavement performance program*. 2003.
26. Tiong, P.L.Y., M. Mustaffar, and M.R. Hainin, *Road surface assessment of pothole severity by close range digital photogrammetry method.* World Appl Sci J, 2012. **19**(6): p. 867-873.
27. Kropáč, O. and P. Múčka, *Classification scheme for random longitudinal road unevenness considering road waviness and vehicle response.* Shock and Vibration, 2009. **16**(3): p. 273-289.
28. Hrovat, D., *Survey of advanced suspension developments and related optimal control applications.* Automatica, 1997. **33**(10): p. 1781-1817.
29. Langdon, J.D., *Design and Adaptive Control of a Lab-based, Tire-coupled, Quarter-car Suspension Test Rig for the Accurate Re-creation of Vehicle Response*, in *Mechanical Engineering*. 2007, Virginia Polytechnic Institute and State University. p. 124.

9 Appendix

The simulation results were obtained for many road obstacle profiles as displayed in the following figures.

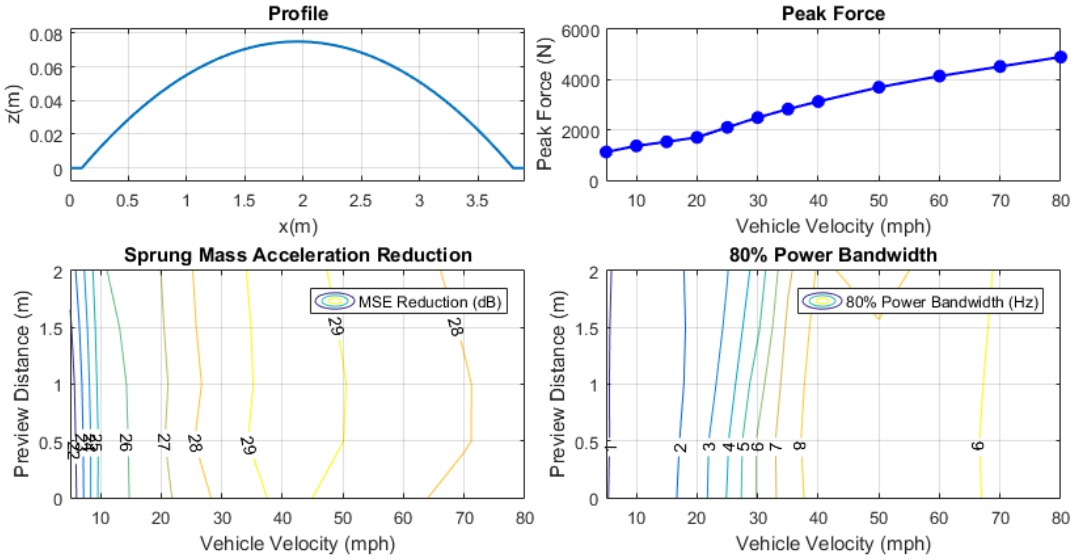

Figure 9.1: Speed Hump Watts Profile

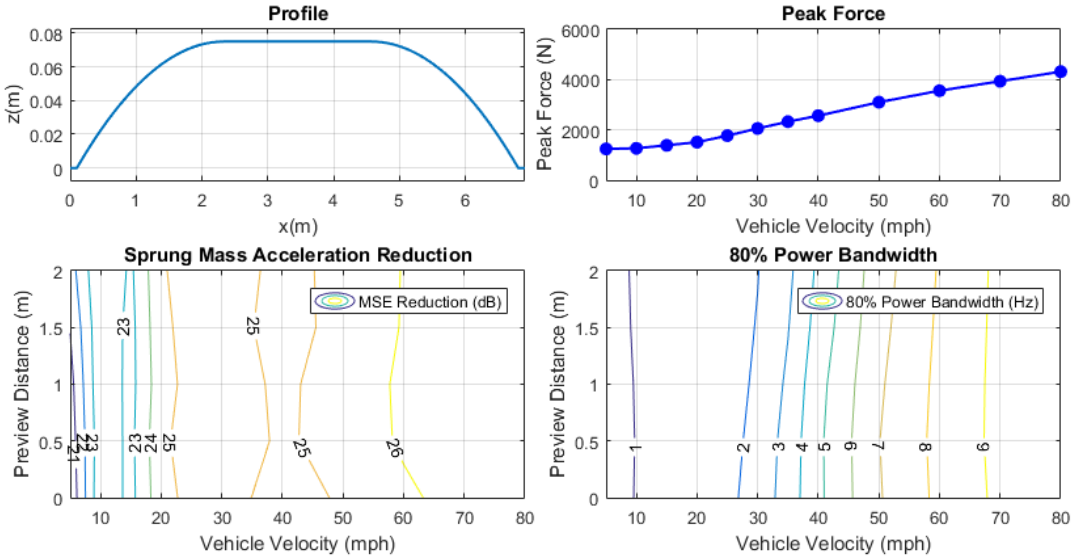

Figure 9.2: Speed Hump Seminole Profile

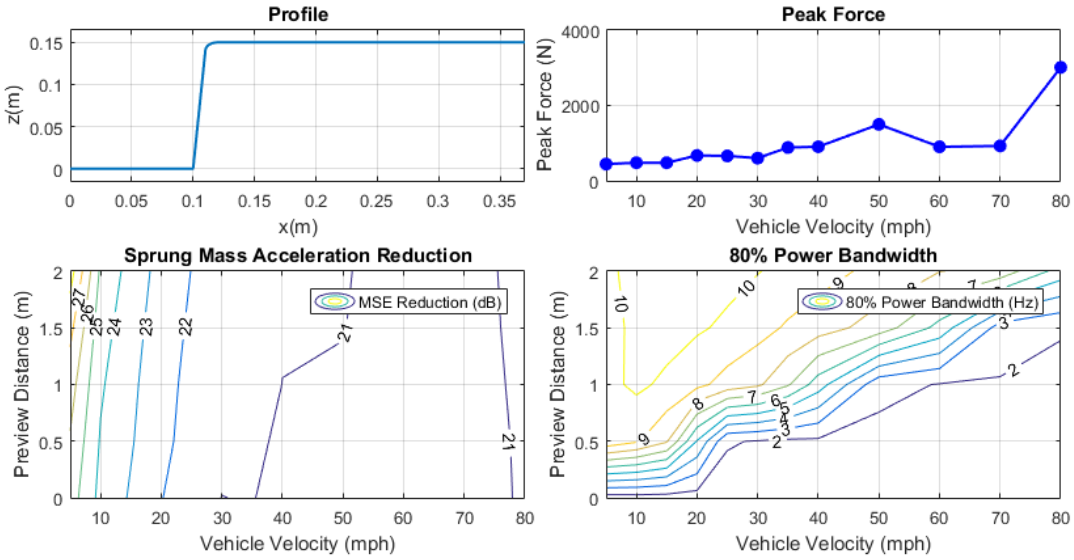

Figure 9.3: Curb A

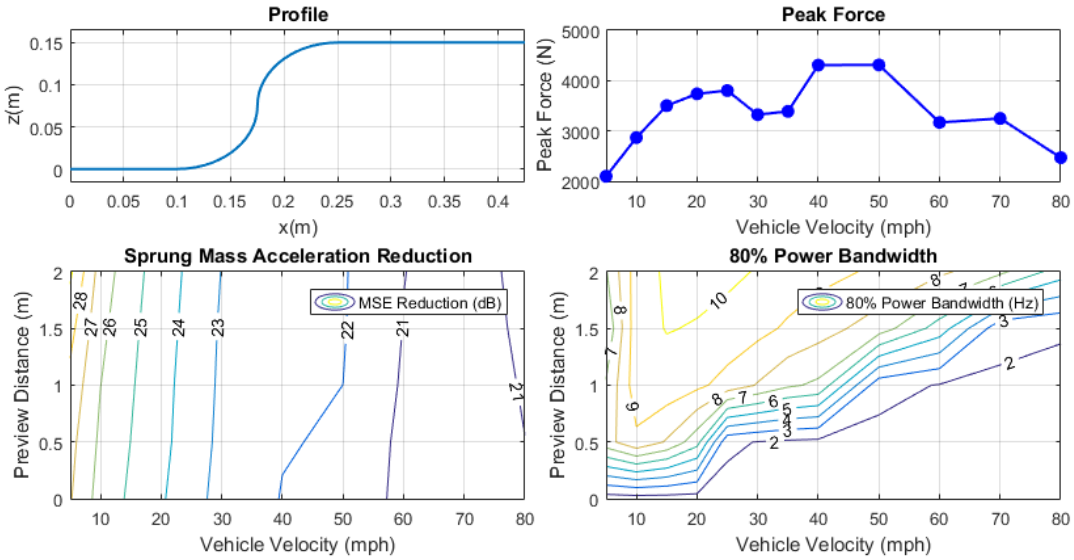

Figure 9.4: Curb B

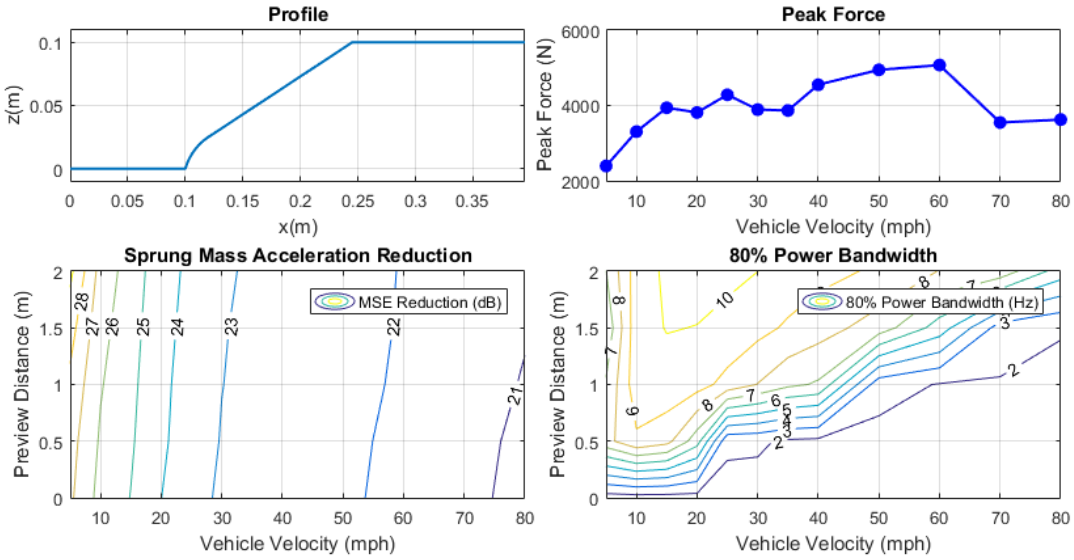

Figure 9.5: Curb C

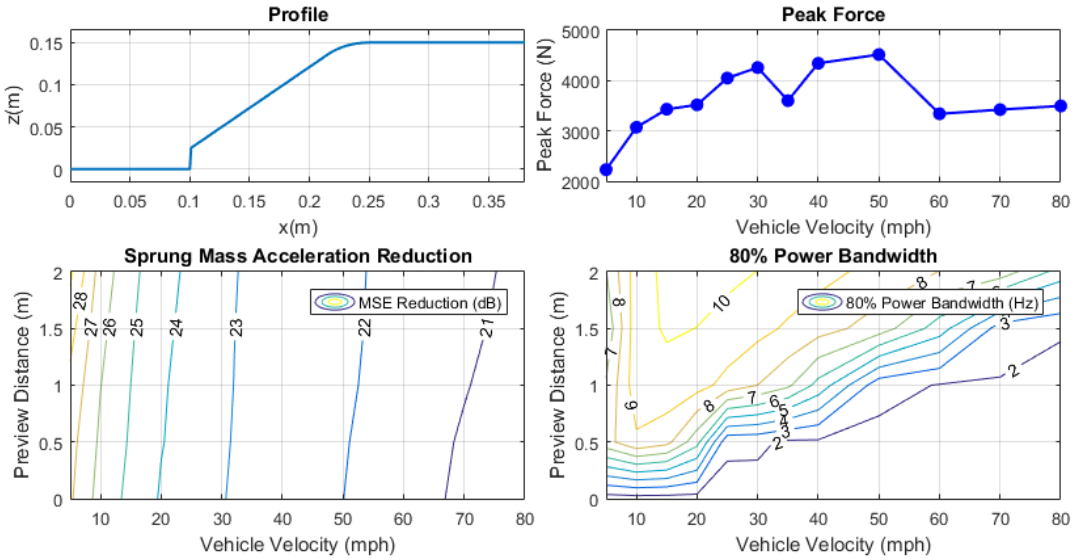

Figure 9.6: Curb D

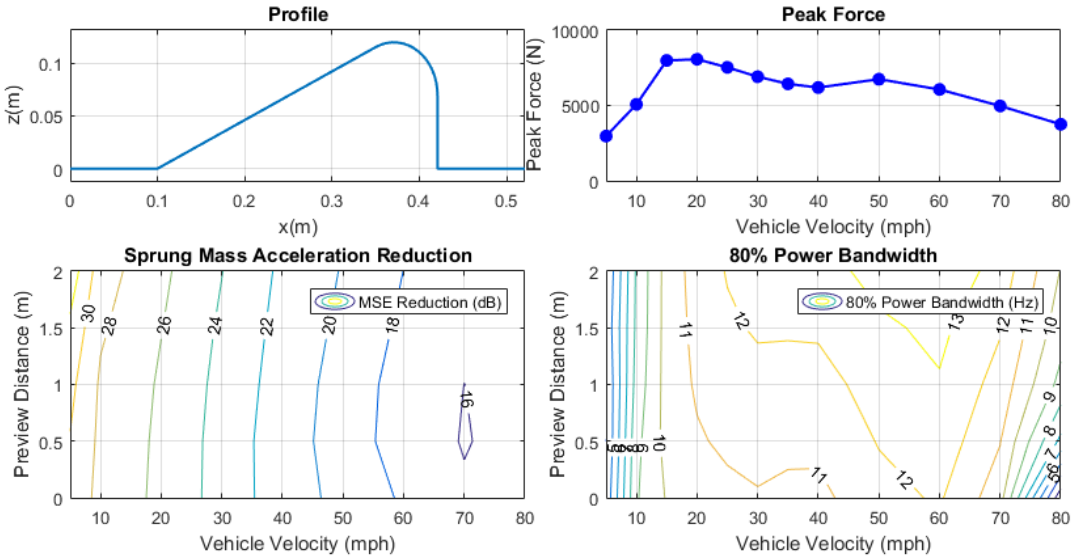

Figure 9.7: Curb E

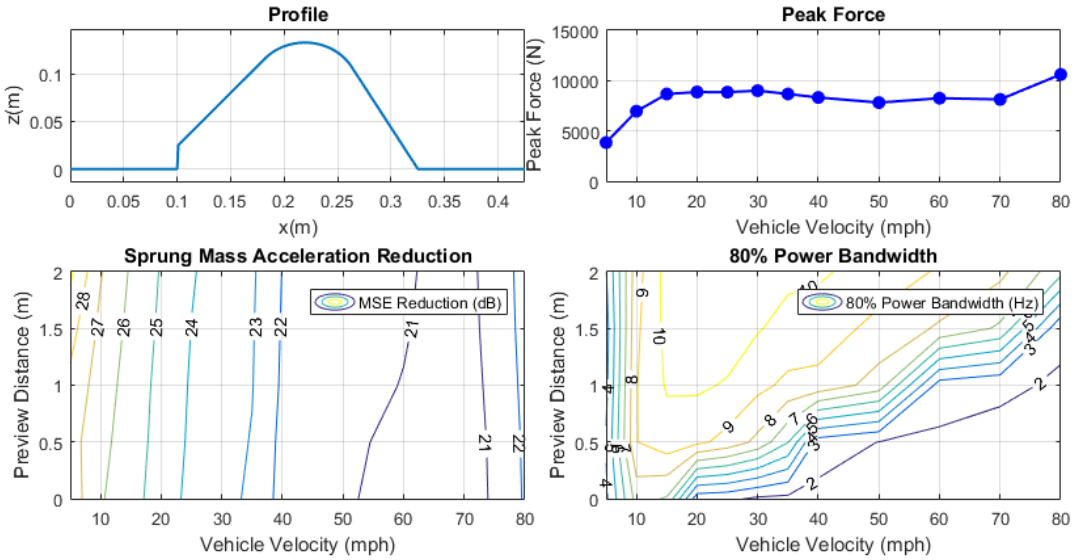

Figure 9.8: Curb F

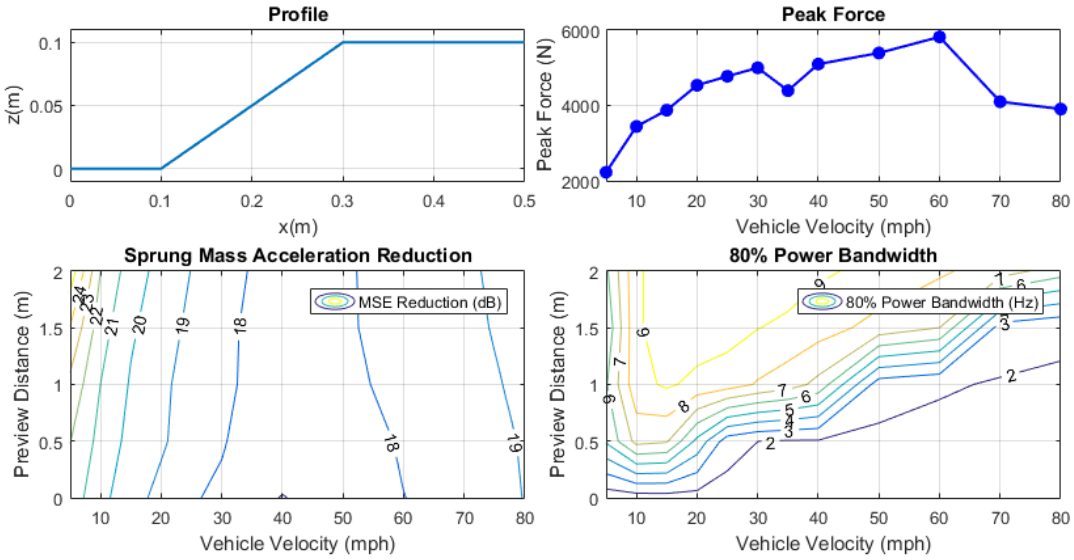

Figure 9.9: Curb G

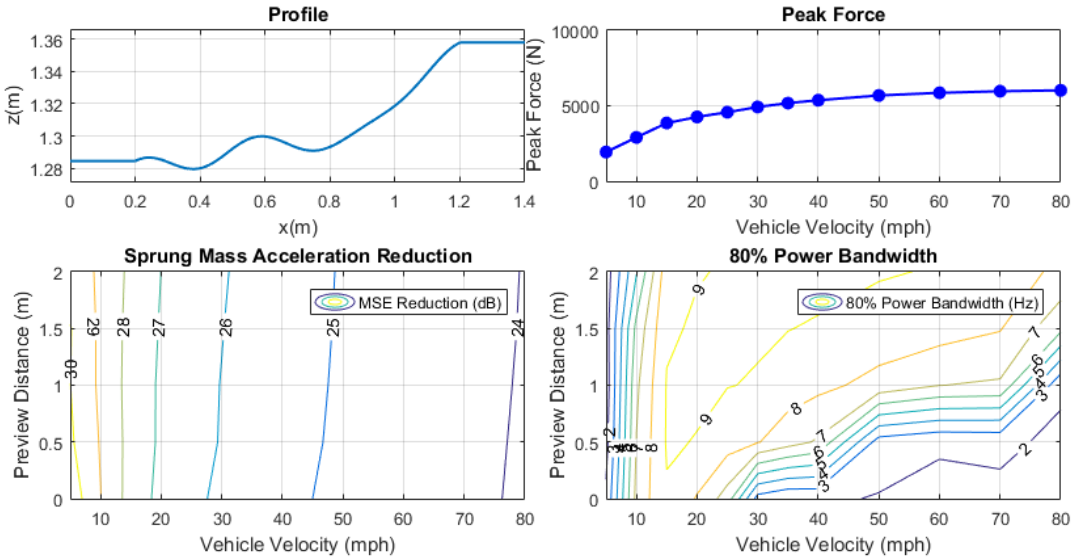

Figure 9.10: Uneven Road A

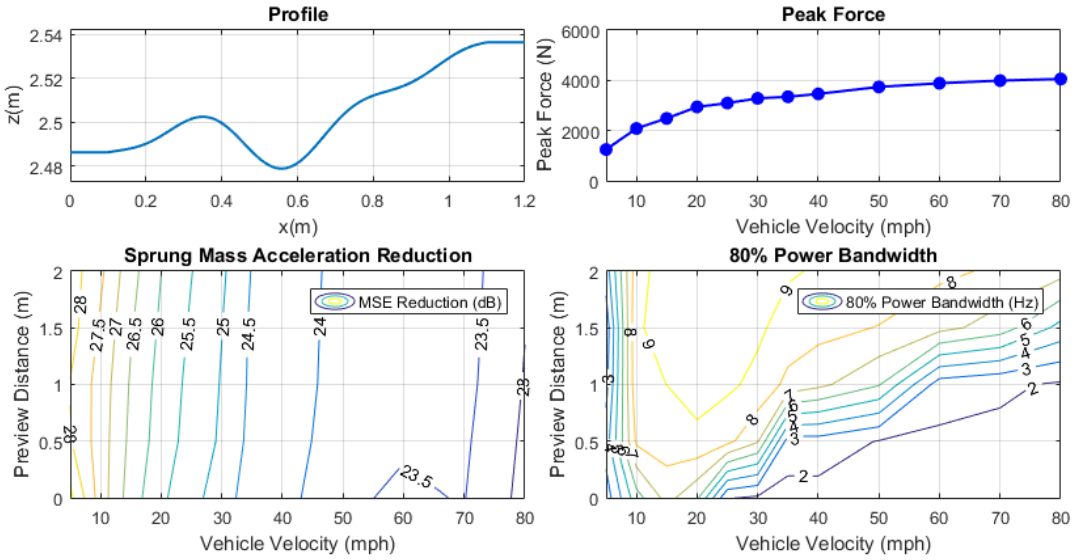

Figure 9.11: Uneven Road B

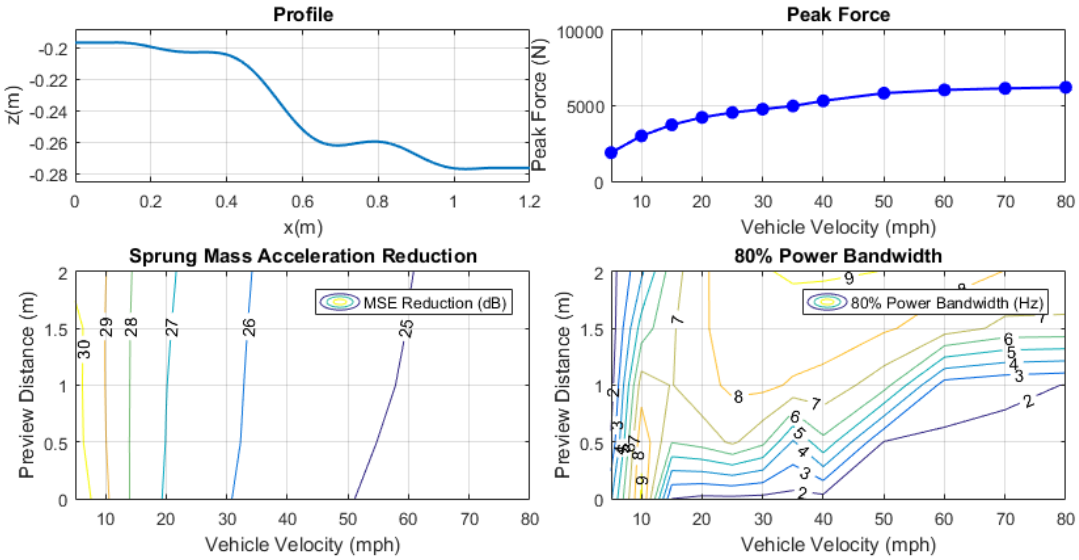

Figure 9.12: Uneven Road C

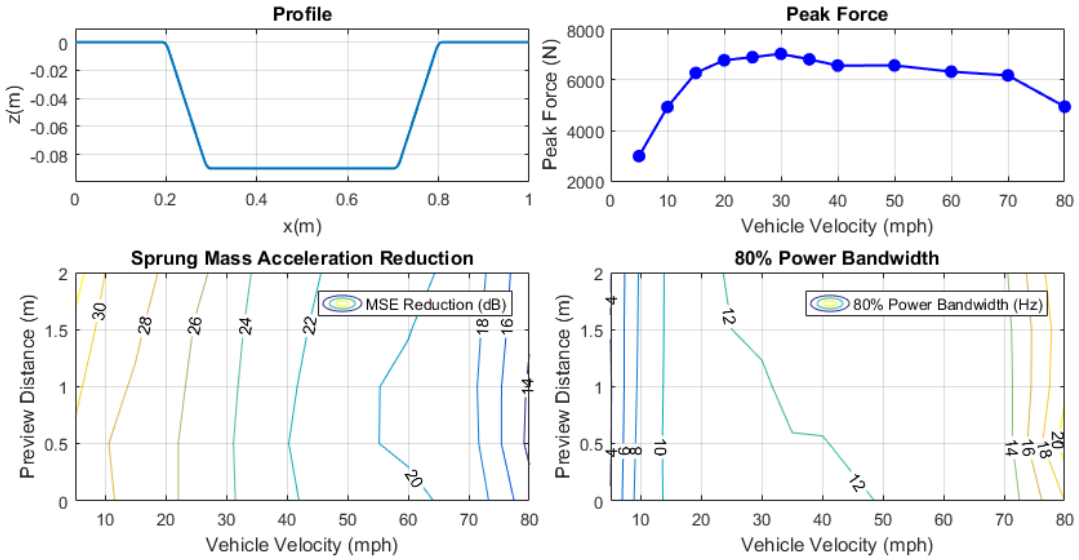

Figure 9.13: Pothole P1

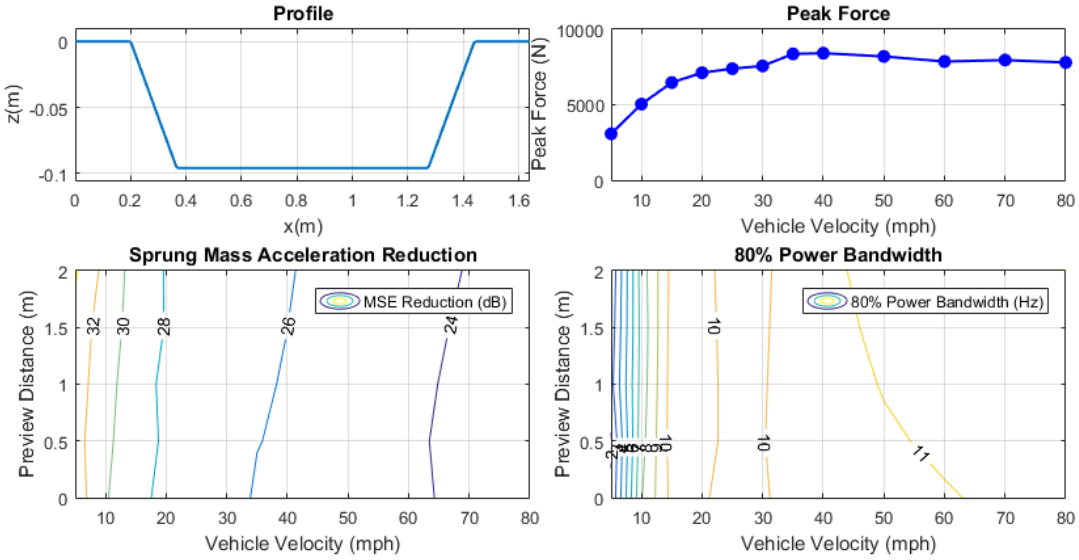

Figure 9.14: Pothole P6

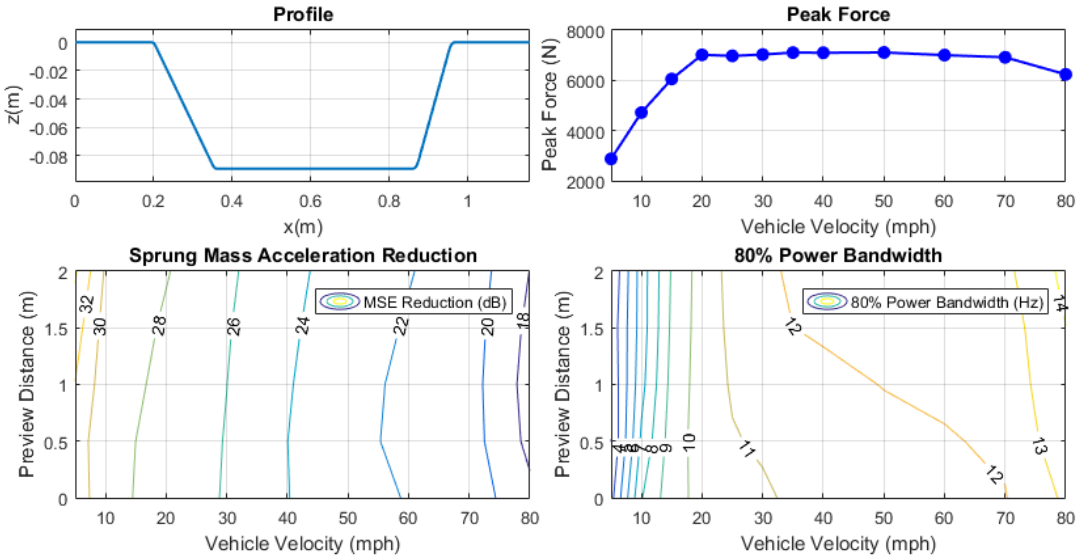

Figure 9.15: Pothole P9